Vortex-induced vibration of a wavy elliptic cylinder

Gustavo R. S. Assi[a,*], Peter W. Bearman[b]

[a] *Dept. of Naval Arch. & Ocean Eng., University of São Paulo, São Paulo, Brazil*
[b] *Department of Aeronautics, Imperial College, London, UK*

Abstract

This paper shows that three-dimensional separation lines on a wavy cylinder may be correlated by the lateral movement of the body responding to flow-induced excitations. Vortex-induced vibration (VIV) of a wavy elliptic cylinder is investigated by mean of experiments in a water channel in the range of Reynold number between 1,500 to 15,000. Results are compared with those for a plain circular cylinder of equivalent diameter with a combined mass-damping parameter of 0.018. Curves of displacement and frequency of vibration showed that the hydroelastic mechanism that drives the wavy cylinder into VIV is not different from that of a plain cylinder. Detailed decomposition of the fluid forces supports this conclusion. The reason for such similar behavior is the correlation of the sinuous separation lines as the wavy cylinder starts to oscillate. Flow visualization reveals that the three-dimensional surface of the wavy cylinder affects the formation of vortices in the near wake, generating streamwise and cross-flow vorticity associated with the wavelength of the surface. However, once the cylinder is free to respond to VIV, moving in the cross-flow direction, coherent vortex filaments once more dominate the near wake.

Keywords: flow-induced vibration, suppression, drag reduction, seal whiskers

1. Introduction

The suppression of vortex-induced vibration (VIV) of bluff bodies with low mass and damping poses a technological challenge faced by many engineering applications. The hydroelastic mechanisms behind the phenomena also generates interesting questions from a scientific point of view. Many different techniques have been proposed to mitigate VIV by controlling the formation of

*Corresponding author: g.assi@usp.br. Address: NDF Research Group – Dept. Eng. Naval e Oceânica, Escola Politécnica da Universidade de São Paulo, Av. Prof Mello Moraes 2231, 05508-030, São Paulo - SP, Brazil. www.ndf.poli.usp.br.

vortices in the near wake. Some methods interfered with the two-dimensional (2D) mechanism of vortex shedding (refer to Assi et al., 2009, 2010a, 2014; Silva-Ortega and Assi, 2017, for examples), interrupting the communication of the separated shear layers as proposed by Gerrard (1966). Others promoted three-dimensional (3D) characteristics of the wake, either by breaking down the dominant vortical features in the near wake or by disrupting the coherent formation or vortices along the span (for example, Cicolin and Assi, 2017). Zdravkovich (1981) presented an interesting overview of many of these techniques, while Rashidi et al. (2016) present a brief review of a few more recent ideas.

The helical strake is the most common device employed by the offshore industry to suppress VIV of riser pipes. Normally, the geometry of the strakes presents three helical blades starting at 120 degrees apart with a common pitch of 5 diameters and a blade height of 20% of the diameter, as seen in figure 1a. As will become clearer, strakes with high blades are required for systems with low mass and damping, which is typical of light elastic structures immerse in water. Elastic structures that are heavy in relation to the displaced mass of fluid (for example, chimneys or bridge cables exposed to wind) are normally fitted with smaller strakes. Helical strakes suffer from an intrinsic problem: while high blades are required to suppress VIV from light structures, they increase drag considerably.

Some researchers have investigated 3D devices other than helical strakes as a means to suppress VIV; we shall recall some of these works in the next section. However, it is worth highlighting now that even though some 3D geometries reduced drag by suppressing vortex shedding from fixed bodies, none has achieved the desired combination of VIV suppression with drag reduction, at least not for systems with low mass and damping.

In the present paper we present an experimental investigation of a 3D cylinder shaped as a *wavy elliptic cylinder* in an attempt to reduce VIV without incurring an unwanted drag penalty. This study will show that the wavy cylinder does not eliminate VIV but it reveals interesting information about the physical mechanisms occurring during the fluid-structure interaction of elastically-mounted 3D bluff bodies.

1.1. Suppression of vortex shedding of fixed cylinders

A relatively simple way to create a slender cylinder with a wavy geometry is by curving its axis in a sinuous path without changing the cross section, as shown in figure 1b. Owen et al. (2000)

and Ahmed (2010), for example, have investigated the flow past a sinuous cylinder of this type. Although this curved body does not have a straight axis, the behavior of the flow separating from the sinuous geometry shows hints of what will happen for 3D bluff bodies with straight axes and varying cross sections.

Owen et al. (2000) performed visualization of the flow at Re = 100 that revealed the intricate wake structures developing from sinusoidal separation lines. Three-dimensional vortex loops appeared correlated with the characteristic wavelength of the geometry. A large periodic variation in the wake structure along the span produced wide wakes at troughs and narrow wakes at peaks, resulting in the disruption of a regular Kármán wake (Owen et al., 1999). A large reduction of 47% in the mean drag was observed compared to that of a 2D circular cylinder. The numerical simulations performed by Darekar and Sherwin (2001) on a square cross-section cylinder with a wavy axis, also at Re = 100, revealed that a rich 3D wake induced by the geometry of the body already exists at low Reynolds numbers. Even though their sinusoidal cylinder had a square cross section, they observed the formation of hairpin vortices similar to those found in the wake of a sphere at low Re.

The model investigated by Ahmed (2010) was slightly different and only presented a single curved section at mid length. The surface topology of the separated flow could be associated with the direction of the incoming flow in relation to a convex or concave configuration of the cylinder. Variations of node, saddle and mixed node-saddle flow attachments produced different 3D flow structures in the near wake. A symmetric shedding of vortices (that had also been observed by Owen et al., 2000) was observed with a saddle type of attachment by Ahmed (2010).

It should be noted that, unlike the geometries to be investigated in this paper, a sinuous cylinder does not present a straight axis. Consequently, the possibility of practical applications for pipes and cables is reduced because it cannot accommodate a straight circular cylinder passing along its centre. In order to allow for this, Owen et al. (2001) reproduced the external waviness on the surface by attaching hemispherical bumps along the span of a plain cylinder. In order to make it an omnidirectional device (one that does not depend on the direction of the incoming flow) they distributed the bumps in a helical pattern around the cylinder, as seen in figure 1c. The model now presents a nearly elliptical cross section at the bumps, which follows a discontinuous helical pattern along the span. As a result, vortex shedding was disrupted by the 3D shape of the body

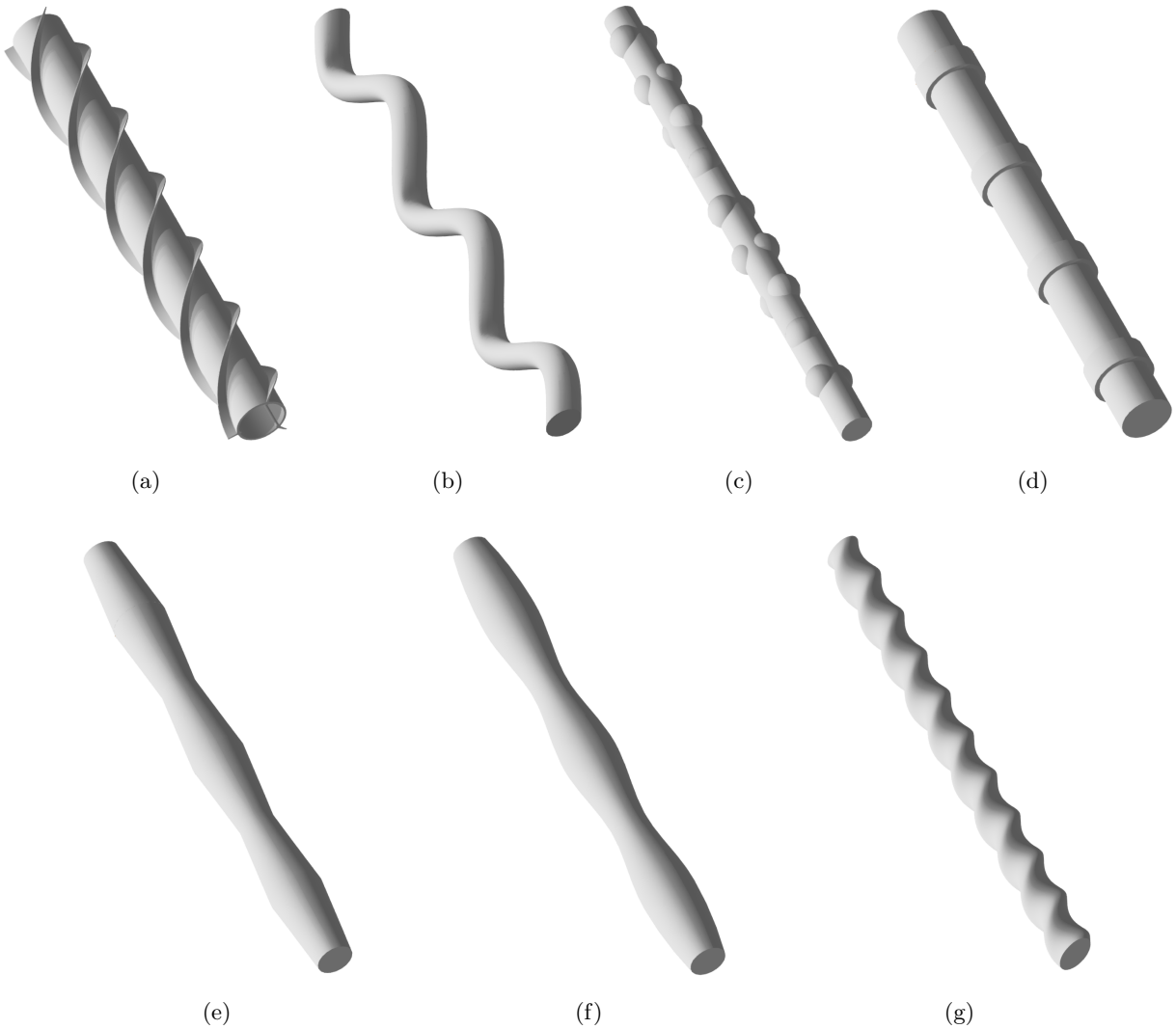

Figure 1: Cylinders with three-dimensional surfaces: *(a)* straight cylinder with helical strakes, *(b)* sinuous cylinder, *(c)* cylinder with bumps, *(d)* cylinder with rings, *(e)* linear-wave cylinder, *(f)* sine-wave cylinder, *(g)* helical elliptic cylinder.

and the mean drag was reduced to $\overline{C_x} \approx 0.9$, roughly a 25% reduction when compared to that of their plain cylinder at Re around 50,000.

While the smooth bumps emulated the waviness of the sinuous cylinder, others have fitted discrete elements to alter the diameter of the body. For example, Nakamura and Igarashi (2008) investigated modifications in the diameter by fitting "cylindrical rings along its span at an interval of several diameters", thus creating the discrete 3D geometric disturbance seen in figure 1d. Rather than observing nodal and saddle attachments associated with the curvature, they verified the formation of separation bubbles near the rings that also produced 3D perturbations in the near wake. The rings induced the formation of vortex loops, resulting in pressure recovery on the rear of the ring. Fluctuating lift acting on the body was was reduced compared to a plain cylinder and a 15% reduction in the mean drag was recorded (Re varying from 3,000 to 38,000).

Bumps and rings have in common a fundamental wavelength associated with their axial distribution along the span. Both Owen et al. (2001) and Nakamura and Igarashi (2008) were able to vary the pitch of their bumps and rings in order to show that there exist optimal configurations to enhance 3D wake disruption and minimize drag.

In an attempt to generate a continuous surface, the discrete rings may be replaced by a linear wave, i. e. creating increasing and decreasing conical slopes along the span with a characteristic wave length (or pitch), as seen in figure 1e. A geometry of this type, with a pitch of about 2 diameters, has been investigated by Zhang et al. (2016) by means of numerical simulations of the flow at $\mathrm{Re} = 5,000$. They found that the "elongated vortex recirculation length led to a larger value of base pressure", which produced a consequent drag reduction of 7% when compared to that of a plain cylinder. In the same study, Zhang et al. (2016) experimented with another 3D shape modification by smoothing out the sloped cylinder into a continuous sinusoidal surface with variable circular cross section, as seen in figure 1f. A further reduction in drag was achieved, with $\overline{C_x}$ reduced by 11% when compared to that of a plain cylinder. (Out of curiosity, Zhang et al. (2016) also investigated a variation of the cylinder with rings, but its performance regarding drag reduction was worse then the others.)

1.2. Wavy cylinders

The experiments of Lee and Nguyen (2007) investigated a wavy cylinder with varying circular cross sections with different wavelengths (as seen in figure 1f) in the range of $\mathrm{Re} = 10^4$. They also

observed that the width of the wake expanded downstream of saddle points and shrunk downstream of node points. Flow visualization revealed strong three-dimensional flow structures related to the geometry of the body. Overall, the vortex formation region was elongated and the vortex-induced fluctuations were suppressed, reducing drag acting on the cylinder by 22% compared with that of a plain cylinder. Zhang et al. (2005) performed PIV measurements of the wake of a similar body at $\mathrm{Re} = 3,000$ and noted that such strong three-dimensional flow structures dominate the wake as far as 5 diameters downstream, with a maximum effect at around 3 diameters downstream of the body. They concluded that organized streamwise vortices with alternating positive and negative vorticity were observed along the span of the wavy cylinder. "They suppress the formation of the large-scale spanwise vortices and decrease the overall turbulent kinetic energy in the near-wake" (Zhang et al., 2005).

New et al. (2013) performed a very detailed study mapping the near wake of wavy cylinders with circular cross section with time-resolved PIV at $\mathrm{Re} = 2,700$. Varying the wave height and length, they concluded that the presence of streamwise vortices associated with saddles and nodes make the near wake less susceptible to other external interferences in the flow, such as aspect ratio and end conditions. They also observed three-dimensional flow structures being more prominent at 3 diameters downstream of the body.

The numerical simulations performed by Lam and Lin (2009) at $\mathrm{Re} = 100$ showed that there might exist optimal values of wave length and height to control the 3D wake and the related drag reduction. For their range of Re the largest drag reductions were achieved for wavelengths between 2.5 and 6 diameters. They noted that the variation of the 3D separation lines along the span resulted in the "development of a three-dimensional free shear layer with periodic repetition along the spanwise direction. The three-dimensional free shear layer of the wavy cylinder is longer and more stable than that of the circular cylinder, and in some cases the free shear layer even does not roll up into a mature vortex street behind the cylinder". As a consequence, drag and lift are significantly reduced.

Experiments conducted by Lam et al. (2004b) at $\mathrm{Re} = 3,000$ to 9,000 characterized the dominant features of the near wake of a wavy cylinder. They also concluded that the average vortex formation length of a wavy cylinder is longer than that of a plain cylinder at the same Re. "For the wavy cylinder, the wake on the saddle plane has a longer vortex formation region and a more

rapid reverse flow, as well as being wider than that on the nodal plane. It was deduced that the free shear layers shed from the points near the saddles extend along the spanwise direction, while the shear layers near the nodes contract." As a result, the wake of a wavy cylinder shows more incoherent structures due to enhanced turbulent mixing. Their measurements were confirmed by visualization of these flow structures at $\mathrm{Re} = 600$.

Ahmed and Bays-Muchmore (1992) performed experiments in a wind tunnel and in a water channel ($\mathrm{Re} = 20,000$) to measure the pressure coefficients around wavy cylinders with various wavelengths (as seen in figure 1f). "Integration of the pressure data revealed greater sectional drag coefficients at the geometric nodes than at the geometric saddles." They also related the formation of streamwise vortices near the nodes with the sinuous three-dimensional separation lines along the wavy cylinder.

In the wind tunnel experiments performed by Lam et al. (2004a), pressure measurements of mean and fluctuating loads were made for three wavy cylinders at Re around 10^4. A maximum 20% drag reduction was observed for the wavy cylinder when compared with that of a plain cylinder. Fluctuating lift was also considerably reduced, indicating that such a geometry could possibly result in VIV suppression. The most interesting result, however, came from measurements of the vortex shedding frequency at various positions along the wavy cylinder. The authors verified that the Stouhal numbers near saddles and nodes are essentially the same. In fact, Strouhal number was found to be approximately 0.2, the same value measured for a plain cylinder.

So far, all the above works dealing with the formation of the wake of a wavy cylinder agreed that the 3D wavy surface of the body significantly modifies the near-wake structure. The vortex-formation length is extended increasing base pressure (thus reducing drag) and the formation of streamwise vortices (with varying intensities) near the nodes is always observed. Similar wake structures are found not only for wavy cylinders with a circular cross section, but also for elongated bodies with wavy trailing edges, as exemplified by Cai et al. (2008) and others.

A very interesting 3D geometry was investigated by Kim et al. (2016), which they called a "helically twisted elliptic cylinder" (seen in figure 1g), by means of numerical simulations of the flow below $\mathrm{Re} = 3,900$. The lowest recorded drag, 23% lower than that of a plain cylinder, was obtained for a twisted cylinder with a wavelength of 3.5 diameters. The authors stated that "the lift fluctuation was zero due to a complete suppression of vortex shedding in the wake".

Jung and Yoon (2014) also investigated the flow about a helical cylinder with an elliptic cross section employing numerical simulations at $\mathrm{Re} = 3,000$. They also found considerable reduction in drag by 13% of that of a plain cylinder, with an almost complete elimination of fluctuating lift. This performance was 5% better than that of a similar wavy cylinder with circular cross section (figure 1f). They verified that the shear layers of the twisted cylinder are more elongated than those of the plain and wavy cylinders, "and vortex shedding from the twisted cylinder is considerably suppressed". As expected to occur for a plain cylinder, they noted that the vortex-formation length of the twisted elliptic cylinders was also reduced with increases in Re.

All previous works mentioned so far have dealt with fixed bluff bodies, i.e. cylinders that were not free to respond to the flow excitation nor forced into oscillatory motion by an external source. The effective reduction of the mean drag of a fixed cylinder with 3D surface is indeed very useful for practical applications in engineering. However, the fact that fluctuating lift was reduced in most cases (sometimes even claimed to have been completely eliminated) does not guarantee that the cylinder will not respond to vortex-induced vibrations. A few researchers attempted to apply cylinders with smooth three-dimensional surfaces to suppress VIV. We shall turn to their work next.

1.3. Vortex-induced vibration

A good device to mitigate fluctuating lift of a fixed cylinder is not necessarily a good device to suppress VIV of a cylinder that is free to respond to the flow. It is well known that the complex fluid-structure interaction happening with an oscillating bluff body may produce a completely different wake when compared to that of a fixed condition (Bearman, 1984). Consequently, the fluid loads exciting a free-to-respond body might also be very different. As it happens for a plain cylinder, the three-dimensional modes occurring in the wake of a fixed circular cylinder described by Williamson (1996) are drastically altered once the cylinder is oscillating, as shown in the works of Blackburn (1998), Hover et al. (2004) and Gioria et al. (2007).

Kleissl and Georgakis (2011), for example, experimented with cylinders with several 3D surfaces as a means to reduce flow-induced vibrations of cables employed in suspension bridges. They found that a wavy-cylinder cover did not increase the mean drag on a cable, but the wavy cylinder could be susceptible to fluidelastic instabilities when Reynolds number approached the critical value associated with the "drag crisis".

Owen et al. (2001) and Bearman and Brankovic (2004) performed VIV experiments fitting a circular cylinder with the bumps presented in figure 1c. They measured the dynamic response of an elastically mounted cylinder with one degree of freedom in the cross-flow direction. Owen et al. (2001) experimented with bumps of various sizes and spacings on a cylinder with a variable mass-damping parameter ($m^*\zeta$ will be properly defined later). For Re $= 1,650$ to 7,500 and $m^*\zeta = 0.036$, they observed a peak amplitude of displacement at the VIV resonance of approximately 0.62 diameters, equivalent to a 25% reduction from the peak response of a plain cylinder. Now, once the mass-damping parameter was increased the peak amplitude of response was significantly reduced. All of their bumps achieved a complete suppression of VIV for $m^*\zeta > 1.5$. At this level of mass and damping a plain cylinder would still be expected to vibrate with displacements of about 0.1 diameters. Their sinuous cylinder also achieved similar results, being able to suppress VIV for $m^*\zeta > 1.0$. Owen et al. (2001) concluded that "when the body is flexibly mounted it is able to detect a very weak force fluctuation" at the resonant frequency; the excitation increases as the response increases.

In the experiments of Bearman and Brankovic (2004) the VIV response of a cylinder fitted with bumps was compared to that of a cylinder fitted with helical strakes (height of 12% of the diameter and pitch of 5 diameters). Reynolds number was up to 10^4 and the combined mass-damping parameter was around $m^*\zeta = 0.006$. While the plain cylinder reached a peak response of 0.9 diameters, the cylinder with bumps reduced the peak vibration by 28% and the straked cylinder by 44%. The height and pitch of the bumps and strakes were comparable, suggesting that the sharp-edged surface of the strakes is indeed required to improve the degree of suppression of VIV.

Very recently, Zhang et al. (2017) performed numerical simulations at $Re = 5,000$ of the VIV of a wavy cylinder with circular cross sections (a geometry similar to that of figure 1f). They concluded that their wavy cylinder presented an "impressive flow control efficacy in the static configuration", with Kármán vortices being "almost eliminated by the span-wise waviness" of the body. However, once the "the wavy cylinder was allowed to move in the transverse direction, the typical lock-in phenomenon still occurred".

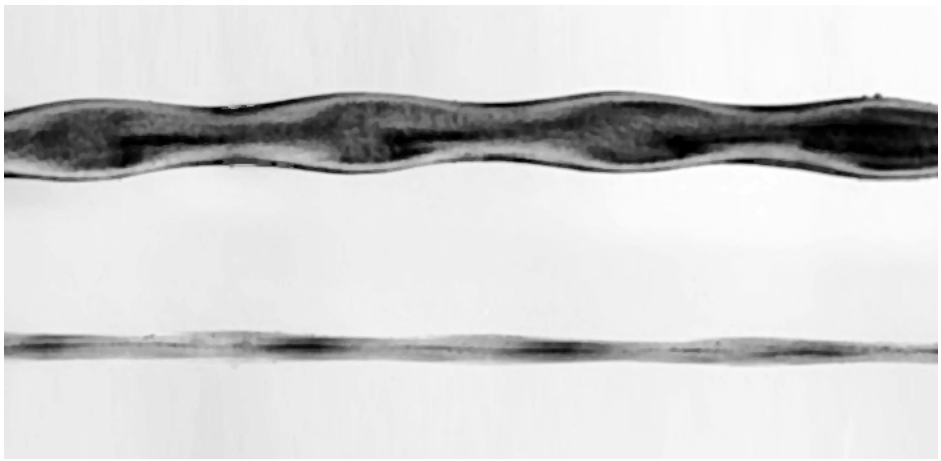

Figure 2: Lateral and frontal views of a section of a harbor seal whisker showing its 3D-wavy surface. Adapted from Hanke et al. (2010).

1.4. Wavy elliptic cylinders in nature

Recently, Beem and Triantafyllou (2015) published an interesting paper on an experimental investigation of the flow-induced vibration of harbour seal whiskers. The seal whisker has a 3D shape that resembles a flattened wavy cylinder. The greater axes of the cross-sectional ellipses are all on the same plane, thus producing a more streamlined geometry to the cross flow approaching from one direction rather then the other orthogonal direction. Hanke et al. (2010), who inspired the geometry employed by Beem and Triantafyllou (2015), presented a clear view of the three-dimensional geometry of the whisker, reproduced here in figure 2. Details on the morphology of seal whiskers, data on their mechanical properties and information on animal behaviour are presented by Ginter et al. (2010), Rinehart et al. (2017) and Hans et al. (2014), among others referred by them.

The natural whisker presents an interesting feature: the undulation of the leading edge (regarding the streamlined direction of the flow) is slightly out of phase with the undulation of the trailing edge. This combination of three-dimensional features produces a bluff body with many of the features discussed above: (i) a curved axis, (ii) waviness in two orthogonal directions (cross-flow), (iii) varying elliptical cross-sections and (iv) smooth surface. Hanke et al. (2010) concluded by experimental and numerical studies of the flow that the seal whiskers "possess a specialized undulated surface structure... that effectively changes the vortex street behind the whiskers and reduces the vibrations that would otherwise be induced by the shedding of vortices". They also

added that "the dynamic forces on harbour seal whiskers are, by at least an order of magnitude, lower than those on sea lion whiskers, which do not share the undulated structure."

Beem and Triantafyllou (2015) explained how the geometry of the whisker is relevant to capture minute fluctuations in the wake present in the upcoming flow, helping the seal to navigate while tracking down its prey. They highlighted that the 3D geometry of the whisker is essential to enhance its ability to sense small pressure fluctuations in the water by allowing it to be induced into wake-induced vibrations (Assi et al., 2010b, 2013) without too much of a drag penalty. In other words, they showed how the whisker "could *slalom* among the vortices of the oncoming wake", making it an efficient sensor. When pure VIV was considered with the flow approaching the streamlined direction of the whisker a minimal response was measured, with a maximum amplitude of displacement of only 0.15 diameters in the cross-flow direction.

1.5. Objective

In the present study we investigate the flow structure of the near wake and the cross-flow response to vortex-induced vibration of an elliptic wavy cylinder with low mass and damping. The present geometry, illustrated in figure 3, shows an elliptical cross section with sinusoidal waviness in both x and y directions. In essence, the geometry is of the same nature as the wavy cylinder with varying circular cross sections discussed above (figure 1f). Nevertheless, the elliptical cross-section produces a geometry with more intense three-dimensional effects along the span.

The current investigation has been developed in the context of finding novel suppressors for the vortex-induced vibration of slender bluff bodies with low mass and damping. Because a successful result of VIV suppression was not achieved (as will be seen in the discussion that follows), we left the data aside with no immediate interest in making it public. However, when the study by Beem and Triantafyllou (2015) on the flow-induced vibration of seal whiskers was published we were surprised by the remarkable similarity between the surface geometries of the seal whisker and that of the elliptical wavy cylinder we had tested years before. We then realized that the results that had been forgotten for a fews years could have been useful as a reference for the VIV response for Beem and Triantafyllou (2015), thus we brought it to light motivated by the topic of bioinspired fluid mechanics.

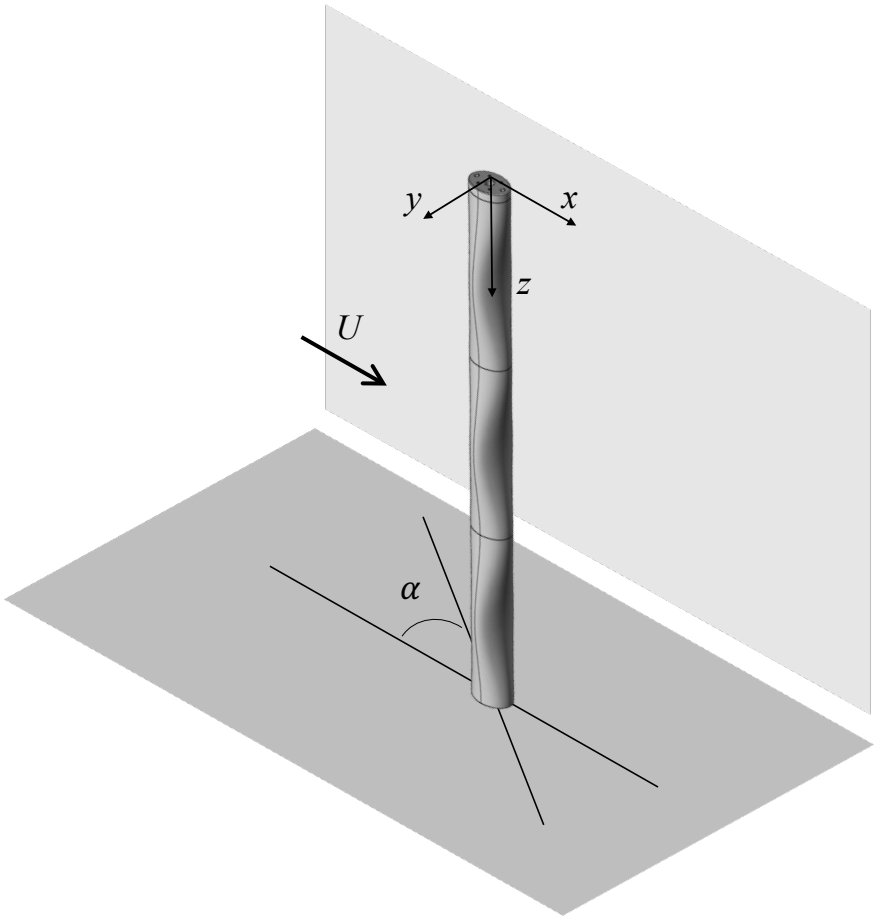

Figure 3: Wavy elliptic cylinder. The angle of attack α represents a positive rotation around the z axis.

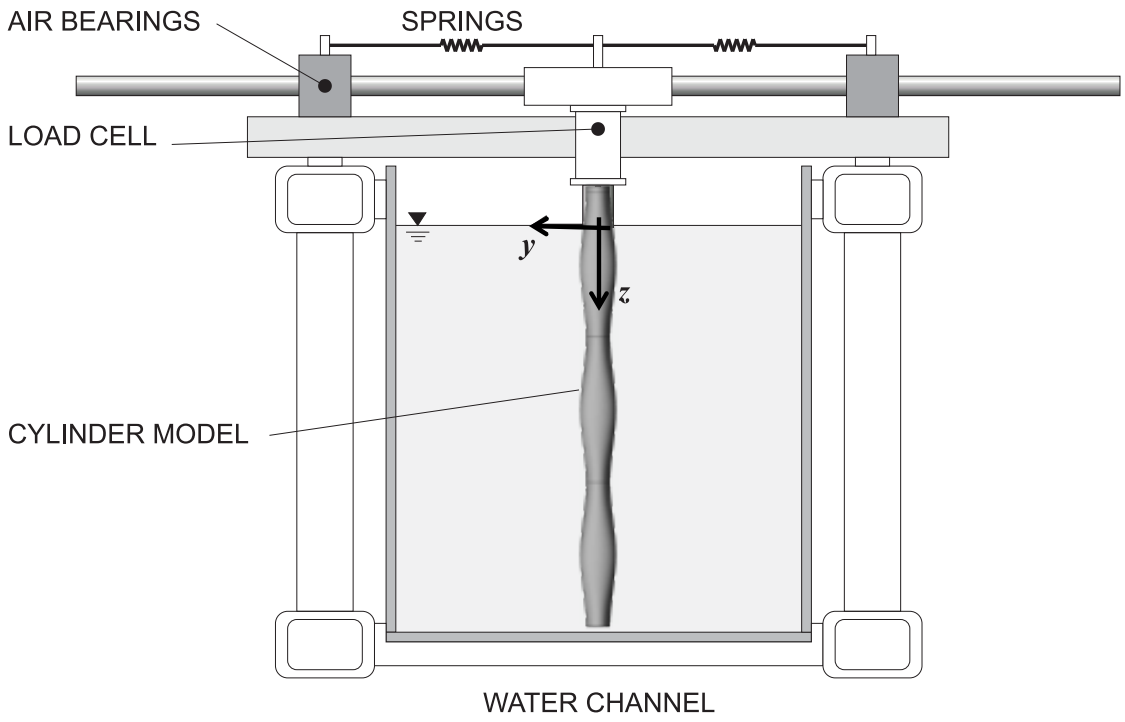

Figure 4: Cross view of the test section.

2. Method

Experiments were performed in the Department of Aeronautics at Imperial College London, UK. Tests were carried out in a free-surface water channel with a test section 0.6m wide, 0.7m deep and 8.0m long. The side walls and bottom of the section were made of glass, allowing a complete view of the models for flow visualization. Flow speed U approaching in the x direction was continuously variable up to 0.6m/s. The maximum free-stream turbulence intensity mapped across the section was around 3% for the range of Reynolds number of the experiments. A cross-sectional diagram of the test section showing the experimental apparatus is shown in figure 4.

An elliptic wavy cylinder was 3D-printed in ABS plastic; the external surface was smoothed and painted black to improve contrast during flow visualizations. Figure 5 presents the geometrical details of the model. The nominal diameter of the cylinder was $D = 50$mm, defined as the average of the larger (60mm) and the smaller (40mm) diameters of the reference ellipse, hence the sinusoidal wave height was 10mm, or 20% of the nominal diameter. The wavelength (also called pitch) was $P = 5D$ and the maximum elliptical ratio of 1.5 occurred at the saddle plane (elongated in the x direction) and at the node plane (elongated in the y direction), marked by the dashed lines

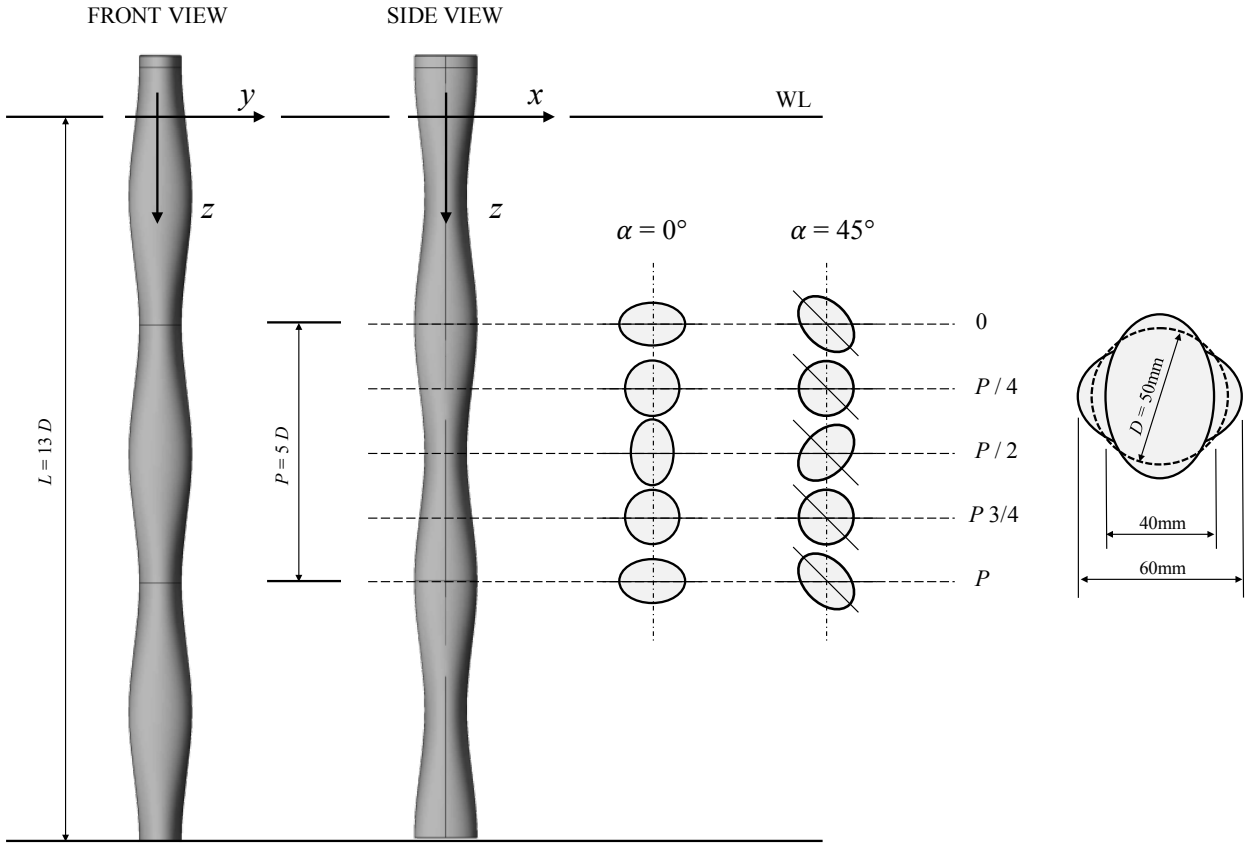

Figure 5: Dimensions of the wavy cylinder. Flow is in the x direction. WL means water line.

at station 0 and $P/2$ in figure 5. The three-dimensional sinusoidal variation between the ellipses resulted in circular cross sections in between the saddles and the nodes at 1/4 and 3/4 of one pitch. The submerged length of the cylinder was $L = 13D$ and the geometric blockage ratio was 8.3%.

The rigid cylinder was connected to a load cell measuring the total instantaneous lift and drag acting on the body. The load cell was attached under an elastic rig supported by two long carbon-fibre tubes sliding through air bearings. The system was free to respond to the flow excitation in the cross-flow (y) direction only; displacements were measured by an optical sensor. The mass ratio, calculated as the ratio between the total structural mass to the mass of displaced fluid, was $m^* = 2.6$. A pair of coil springs provided the stiffness of the system. The natural frequency of oscillation (f_0) as well as structural damping were determined during decay tests performed in air, hence not taking into account hydrodynamic effects. The structural damping ratio was kept to a minimum value of $\zeta = 0.7\%$, calculated as a percentage of the critical damping during decay tests performed in air. The resultant combined mass-damping parameter was $m^*\zeta = 0.018$.

The only flow variable changed during the course of the experiments was the flow velocity U, which altered both the Reynolds number between 1.5×10^3 and 1.5×10^4 ($\mathrm{Re} = UD/\nu$, where ν is the kinematic viscosity of water and D is the nominal diameter) and the reduced velocity (U/Df_0) in the range of 2 to 16. The dynamic response to VIV was analyzed across the reduced velocity range by comparing the normalized amplitude of displacement ($\hat{y}/D$, where $\hat{y}$ is the RMS of y times $\sqrt{2}$) and the dominant frequency of oscillation normalized by the natural frequency (f/f_0). Fluid forces and other parameters derived from them have been calculated from the measurements obtained with the load cell. A plain circular cylinder with the same D, mass and damping parameters has also been tested to provide a reference response for VIV.

Since the elliptic wavy cylinder is not axisymmetric, experiments with two orientations regarding the incoming flow have been performed, as illustrated in figures 3 and 5. First the larger axis of the ellipse at the saddle plane was aligned with the direction of the flow, defining an angle of attack of $\alpha = 0^\circ$ in relation to U. A second configuration was obtained by rotating the cylinder by 45° around the z axis, resulting in $\alpha = 45^\circ$. Results for both configurations are compared with those for a plain cylinder in the next section.

2.1. Flow visualization

In the present experiment, visualization of the flow by means of fluorescent dye has been performed by painting the front of the model with a solution of rhodamine, alcohol and corn syrup. Dissolved dye convected by the flow was illuminated with ultra-violet light and laser sheets. This technique allowed for a clear visualization of the separation lines along the surface of the body, but the dye tracers quickly diffused as soon as they reached the more turbulent regions of the wake.

In order to highlight the flow features in the near wake, flow visualization was also performed by means of hydrogen bubbles emitted by the electrolysis of water from two thin wires stretched parallel to the vertical axis of the cylinder. The wires were placed at about one diameter upstream of the body and slightly off the centerline of the wake. When the cylinders were oscillating, the lateral position of the wires was adjusted more to the side, so that a curtain of bubbles would reach the body during vibration. This technique allowed for visualization of the three-dimensional vortex structures present in the wake for about a distance of 7 cylinder diameters downstream.

Both techniques were performed at a Reynolds number of $3,000$ for $\alpha = 0^\circ$ and 45°, in which the wake is already fully three-dimensional (also near the peak response of VIV). While a good understanding of the flow features was obtained by observing the flow in the water channel, recorded images and movies were not of sufficient graphical quality to be reproduced in this paper. Therefore, the dominant flow features in the near wake are illustrated by means of the sketches and diagrams originated from careful observation by the naked eye while the experiments were running.

3. Results and discussion

The first series of experiments was performed with fixed cylinders by restricting the movement of the elastic rig. The total drag coefficient, obtained by non-dimensionalizing the total drag force by $\frac{1}{2}\rho U^2 DL$, employed the nominal diameter D. The mean part of the total drag coefficient ($\overline{C}_x$) is presented in figure 6. The mean drag for the reference plain cylinder varied around $\overline{C}_x = 1.04$ for the Re range of the experiment, with a maximum value of $\overline{C}_x = 1.21$ and a minimum of 0.81, which are in agreement with other works in the literature (Zdravkovich, 1997, for example). Other effects, due to free stream turbulence intensity (Bell, 1983) or cylinder aspect ratio (Zdravkovich et al., 1989), for example, may contribute to change the mean drag from the canonical value expected

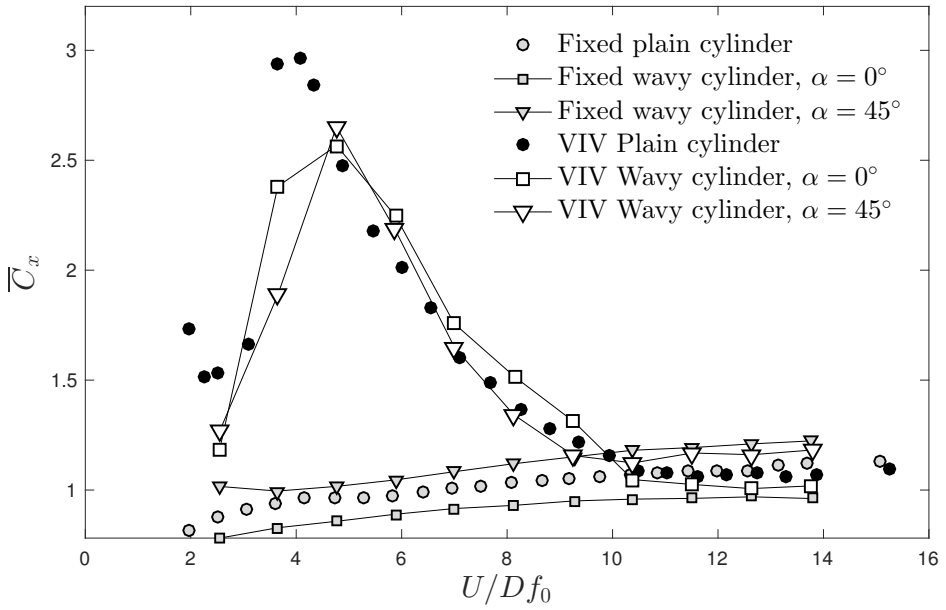

Figure 6: Mean drag measured for fixed and oscillating cylinders.

for a two-dimensional body. Nevertheless, since all models have been measured under the same condition, this value of $\overline{C}_x$ for a plain cylinder will be taken as a reference for comparison.

The wavy cylinder at $\alpha = 0°$ presented a lower mean drag for the same conditions, with a consistent reduction by 12.5% throughout the Re range when compared with the $\overline{C}_x$ of the plain cylinder. The wavy cylinder at $\alpha = 45°$, on the other hand, presented an increase of $\overline{C}_x$ of about 7% when compared with that of the plain cylinder. In relation to the $\alpha = 0°$ configuration, $\overline{C}_x$ for $\alpha = 45°$ was increased by an average of 22%.

One should bear in mind that C_x was calculated using the nominal diameter D of the body. While both the plain cylinder and the wavy cylinder at $\alpha = 0°$ have the same frontal area, the wavy cylinder at $\alpha = 45°$ presents a projected frontal area increased by around 1%. If the increase in the effective diameter is taken into account in calculating C_x, the mean drag of the wavy cylinder at $\alpha = 45°$ would still be roughly at the same level. Therefore, the significant drag reduction experienced by the wavy cylinder at $\alpha = 0°$ is indeed of a hydrodynamic nature, and not simply due to an area change. As far as the flow is concerned, the three-dimensional effects of the surface affecting the near wake are not as pronounced at $\alpha = 45°$ as they were at $\alpha = 0°$. In other words, the elliptic wavy cylinder at $\alpha = 45°$ "appears less three-dimensional" to the flow. For the sake of comparison, we shall keep all hydrodynamic coefficients in the present work non-dimensionalized

by the nominal diameter D.

Bearman and Owen (1998) and others cited above attributed the drag reduction to the increase of base pressure created by the 3D shape of the separation lines. Flow visualization supporting this idea will be discussed later in this paper.

3.1. Response to vortex-induced vibration

The response to VIV has been determined by increasing the flow speed (U) and keeping all other parameters constant. Figure 7a presents the harmonic amplitude of displacement for the whole range of reduced velocities tested. The typical response of a plain cylinder was characterized by a build-up of vibration during the synchronization range between $U/Df_0 \approx 3$ and 11. A maximum response of $\hat{y}/D = 0.82$ has been observed at the peak of resonance in the upper branch. The dominant frequency of oscillation, presented in figure 7b, shows the departure of the frequency curve from the $St = 0.2$ line towards $f/f_0 = 1$ during the synchronization range, also called the lock-in range. These results are in good agreement with many other results presented in the literature regarding the cross-flow VIV of rigid cylinders with low mass and damping (Bearman, 1984; Williamson and Govardhan, 2004, for example). When comparing the current results with others in the literature, please bear in mind that the synchronization range might be shifted to lower reduced velocities because f_0 was measured in air and not in still water.

Figure 7 also presents the VIV response for the two configurations of the wavy cylinder. There is no significant difference between the responses of the wavy cylinder at $\alpha = 0°$ and 45° in figure 7a. The width of the synchronization range for the wavy cylinders is just slightly reduced when compared with that of the plain cylinder and the peaks of response at resonance reach $\hat{y}/D = 0.87$ and 0.93 for $\alpha = 0°$ and 45°, respectively. The frequency signatures seen in figure 7b are also very similar to that of the plain cylinder.

Even though the wavy cylinder at $\alpha = 0°$ presented a considerably lower mean drag than the wavy cylinder at $\alpha = 45°$, their responses to VIV are practically identical. If fact, as far as the response is concerned, both wavy cylinders behaved very similarly to the plain cylinder, suggesting that the hydroelastic phenomenona driving the oscillations (i.e. the interaction of the oscillating cylinders with an organized Kármán wake) are the same in nature and comparable in intensity.

When both wavy cylinders were held fixed, differences in the flow structures contributed to increased drag for $\alpha = 45°$ and reduced drag for $\alpha = 0°$. Now that the cylinders are oscillating,

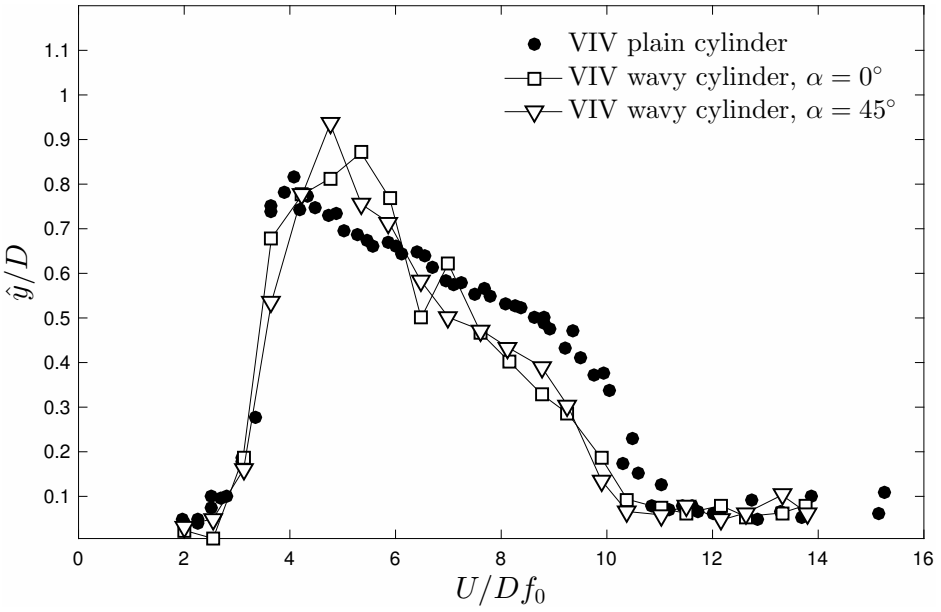

(a)

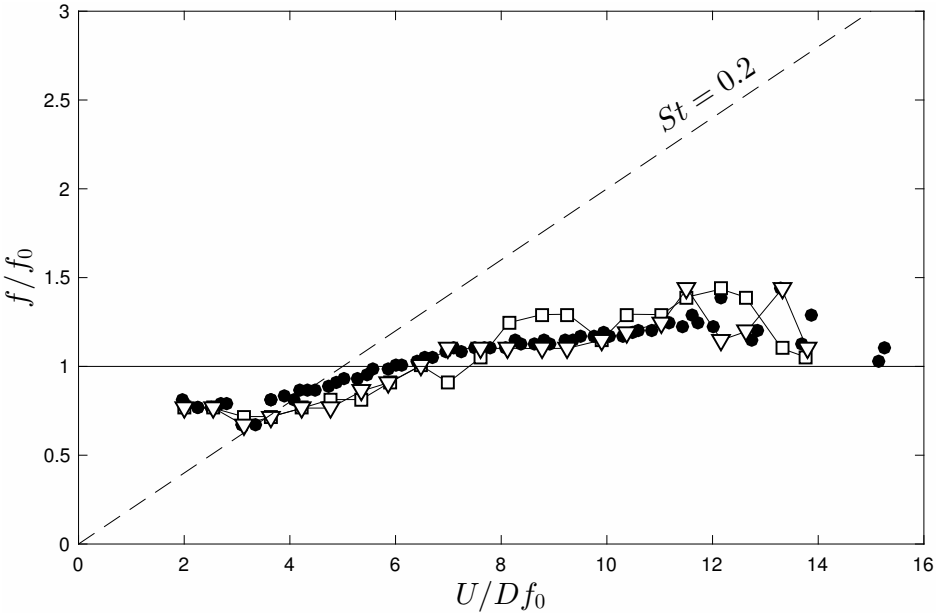

(b)

Figure 7: *(a)* Amplitude of displacement and *(b)* dominant frequency of vibration versus reduced velocity.

it appears that there is no difference in the hydrodynamic effects occurring for the wavy cylinders from the plain cylinder. As seen in figure 6, even the mean drag during VIV followed the same behavior for all three cases. We will argue that the different flow structures found for the three fixed bodies (especially concerning the 3D separation lines) are made the same when the bodies start to oscillate in the cross-flow direction.

3.2. Fluid forces

The hydroelastic system, allowing for displacements only in one degree of freedom in the y-axis, can be modelled by

$$m\ddot{y} + c\dot{y} + ky = C_y(t)\frac{1}{2}\rho U^2 DL, \tag{1}$$

$$y(t) = \hat{y}\sin(2\pi f t), \tag{2}$$

where y, $\dot{y}$ and $\ddot{y}$ are respectively the displacement, velocity and acceleration of the body and $C_y(t)$ is the time-dependent force coefficient in the cross-flow direction.

Following Bearman (1984), $y(t)$ of a cylinder under VIV may be expressed by the harmonic response of a linear oscillator, with $\hat{y}$ and f respectively representing the harmonic amplitude and frequency of oscillation. The fluid force and the body response oscillate at the same frequency f, which is usually close to the natural frequency of the system for large-amplitude oscillations under a steady-state regime of VIV. According to this 'harmonic forcing and harmonic motion' hypothesis the lift coefficient can be divided into a time-average term $\overline{C}_y$ and a transient term modelled as a sine wave with amplitude $\hat{C}_y$. Hence

$$C_y(t) = \overline{C}_y + \hat{C}_y\sin(2\pi f t + \phi), \tag{3}$$

where ϕ is the phase angle between the displacement and the fluid force. For body excitation to occur, the phase angle between displacement and fluid force must be between $\phi = 0°$ and $180°$. A phase angle equal either to $0°$ or $180°$ means that no energy is transferred from the fluid to the structure to excite any vibration.

Figures 8 and 9 show examples of the time series of instantaneous displacement (y/D) and lift coefficient (C_y) measured for a few cycles of oscillation of the wavy cylinders at four different reduced velocities. Again, there are no significant differences between $\alpha = 0°$ and $45°$. In both cases, one may note a very well behaved harmonic curve of displacement in response to an also

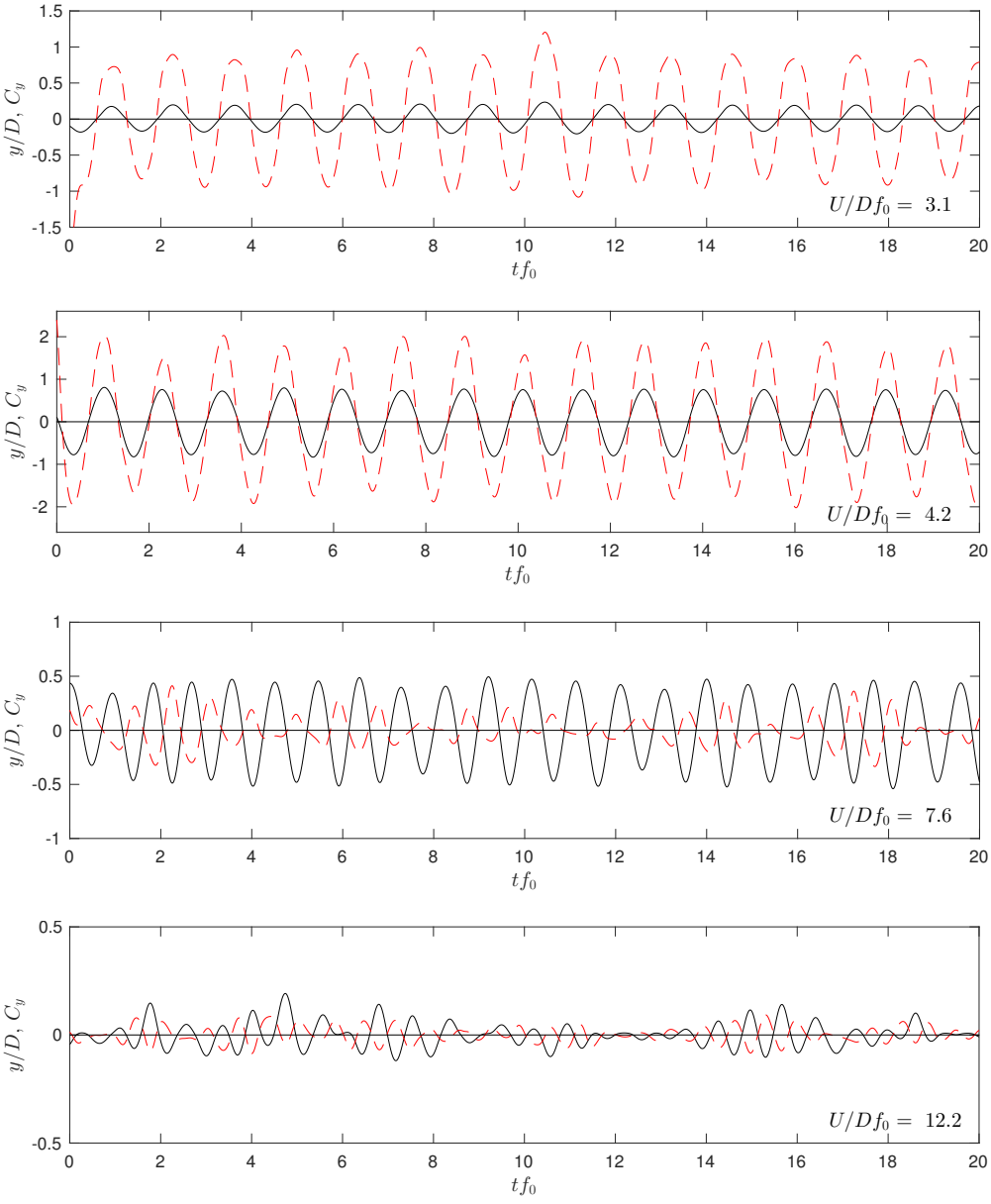

Figure 8: *Colour online.* Time series of displacement (continuous line) and lift coefficient (dashed line) for a wavy cylinder at $\alpha = 0^\circ$.

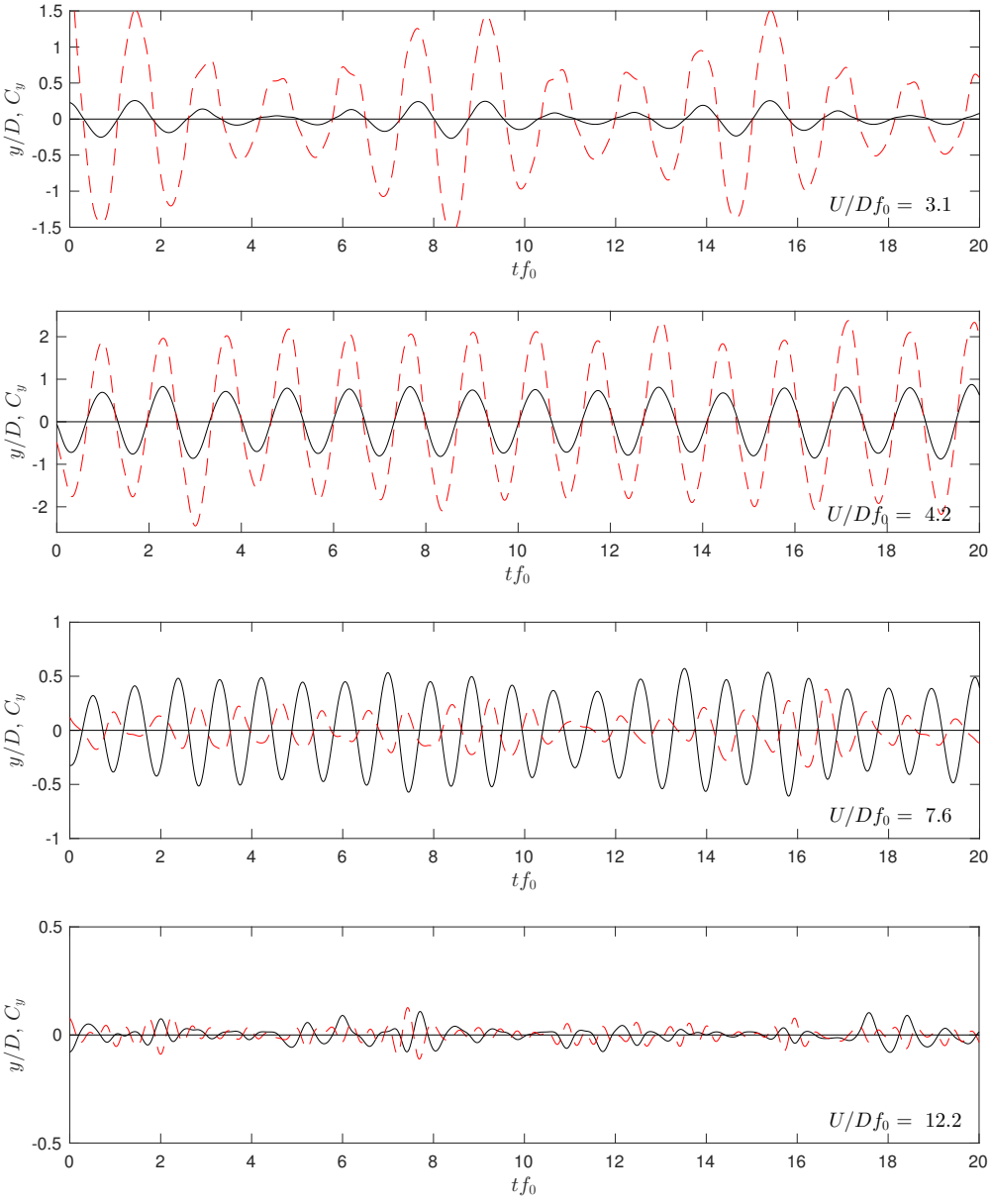

Figure 9: *Colour online.* Time series of displacement (continuous line) and lift coefficient (dashed line) for a wavy cylinder at $\alpha = 45^{\circ}$.

well behaved lift curve. For reduced velocities below the resonance peak at $U/Df_0 \approx 5$, y and C_y appear to be almost in phase. For reduced velocities beyond the resonance peak, y and C_y appear to be almost out of phase. Nevertheless, it is evident that both y and C_y have the same dominant frequency, thus supporting the use of the harmonic models proposed above.

Figure 10a presents the RMS of the lift coefficient ($\tilde{C}_y$) for the wavy cylinders compared with that of the plain cylinder. The similarity between the three curves is remarkable. The range of increased $\tilde{C}_y$ of the plain cylinder corresponding the the synchronization range of VIV is matched by the wavy cylinders. The intensities of $\tilde{C}_y$ are also of comparable values.

In the present work, ϕ is estimated directly from the measurements of displacement and lift, by calculating

$$\phi = \arccos R_{(y,C_y)}, \tag{4}$$

between both signals, where $R_{(y,C_y)}$ is the coefficient of cross-correlation between y and C_y. Bearman (1984) states that "It is clear that the phase angle ϕ plays an extremely important role. The amplitude response does not depend on $\hat{C}_y$ alone but on that part of $\hat{C}_y$ in phase with the body velocity. Hence, measurements of the sectional fluctuating lift coefficient on a range of stationary bluff-body shapes will give little indication of the likely amplitudes of motion of similar bodies flexibly mounted".

Figure 10b presents ϕ versus reduced velocity for the three cases. The phase shift corresponding to the system passing through resonance is experienced in the same way by all three models. Please bear in mind that residual vibrations beyond the synchronization range (for $U/Df_0 > 11$) are due to turbulence buffeting; they present small amplitudes near the natural frequency, hence ϕ is not properly defined because the harmonic assumption does not hold there anymore.

As shown by Khalak and Williamson (1999) and others for plain cylinders with low $m^*\zeta$, the shift of almost 180° in ϕ is associated with a change in the mode of vortex shedding. That is to say that the response of the structure is strongly dependent on the vortex shedding mechanism, and vice versa, within the synchronization range. This emphasizes the importance of the phase angle between y and C_y in transferring energy into the system to sustain different regimes of VIV.

Figure 11 presents the power spectra of the normalized frequency of oscillation (f/f_0) and the frequency of the lift force (f_{C_y}/f_0) for the wavy cylinder at $\alpha = 0°$ and 45° versus reduced velocity. The darker shades represent peaks of the power spectra, normalize by the value of the maximum

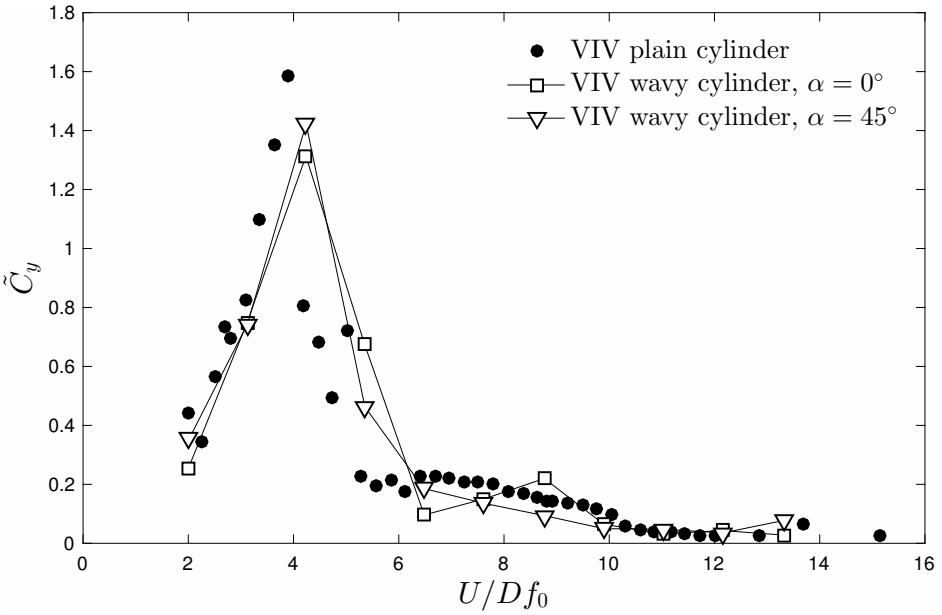

(a)

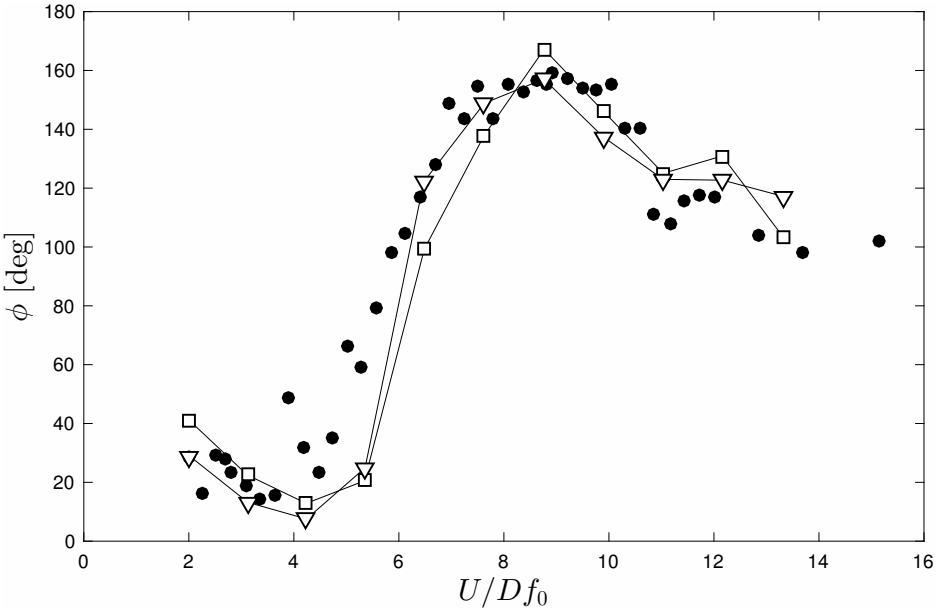

(b)

Figure 10: *(a)* RMS of lift coefficient and *(b)* phase angle between lift and displacement.

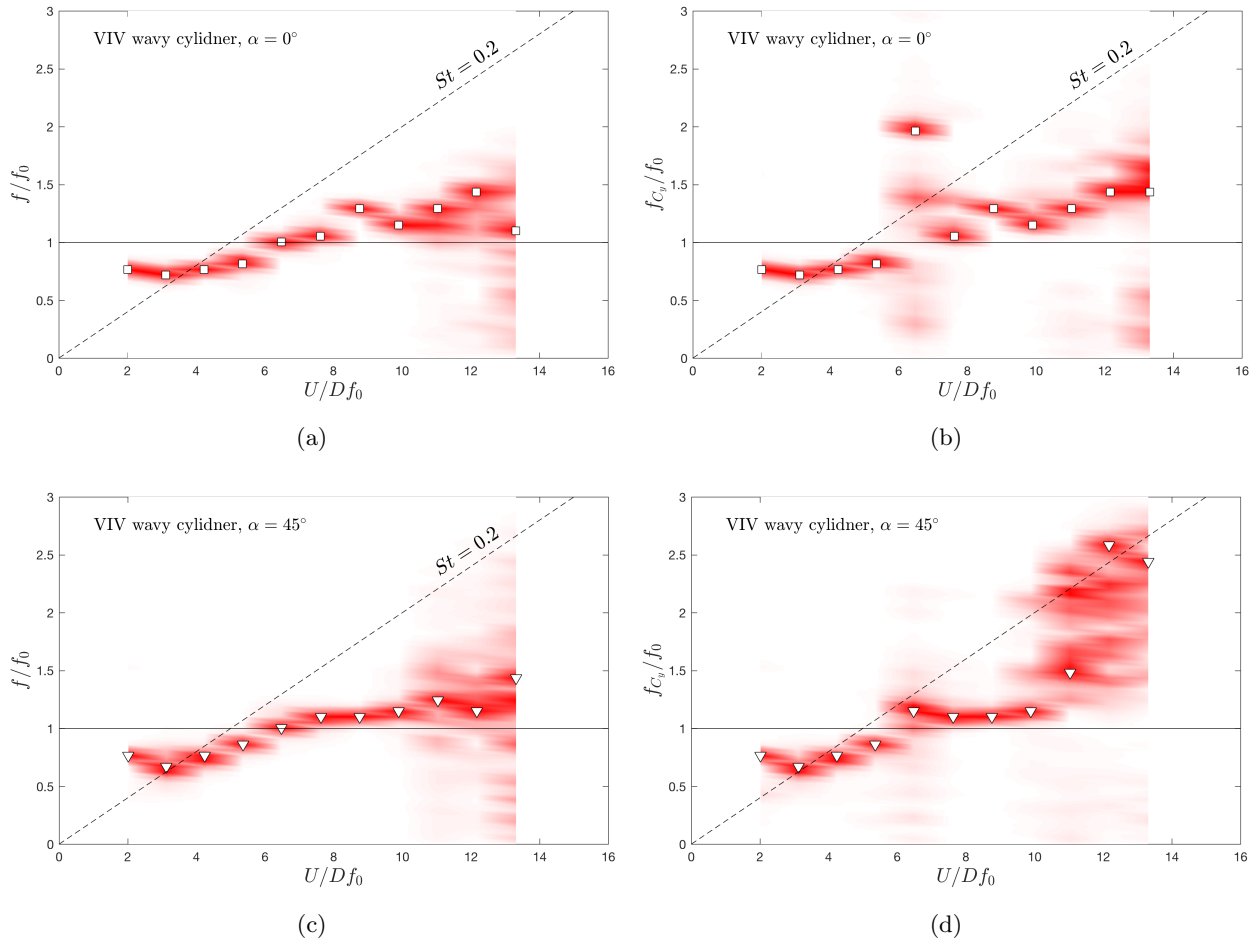

Figure 11: *Colour online.* Power spectra of the frequency of oscillation (f/f_0) and the frequency of the lift force (f_{C_y}/f_0) versus reduced velocity.

peak at each reduced velocity. The dominant frequencies for each reduced velocity are marked with symbols, hence symbols in figures 11a and 11c representing f/f_0 are those shown in figure 7b.

For both $\alpha = 0°$ and $45°$, f/f_0 showed a pretty clear signature with a single dominant frequency for the whole of the synchronization range. The spectra of f_{C_y}/f_0 also showed a clear signature, with only a broader spectrum at $U/Df_0 \approx 6$, near the transition from the upper to the lower branch of VIV. This might be associated with the intermittent or chaotic transitions between branches, as suggested by Khalak and Williamson (1999) to be occurring for plain cylinders, but one cannot be more conclusive only with the available data. For $U/Df_0 > 11$, beyond the synchronization range, the excitation presented a much broader spectrum, especially for $\alpha = 45°$, with the dominant f_{C_y}/f_0 reaching the $St = 0.2$ line. The response, on the other hand, appears with dominant f/f_0 near the natural frequency, an indication of turbulence buffeting.

These results concerning the response and the driving force (figures 7 and 10) already offer evidence to show that the wavy cylinder is simply responding to VIV, driven by the same mechanism as a plain cylinder. However, in order to support this hypothesis and provide data for the comparison with future investigations, we shall briefly discuss other parameters to highlight the physical principles behind the excitation.

Figure 12a presents the $C_y \cos\phi$, the part of the lift coefficient in phase with the body acceleration that takes the form of a fluid-dynamic inertia, therefore closely related to the actual frequency of oscillation. As expected to occur for the plain cylinder, $C_y \cos\phi$ found a peak at the VIV resonance followed by negative values corresponding to the lower branch. The behavior observed for the two wavy cylinders was not different.

In the review presented by Williamson and Govardhan (2004), an "effective added mass" coefficient is defined by

$$C_{EA} = \frac{1}{2\pi^3} \frac{C_y \cos\phi}{\hat{y}/D} \left(\frac{U}{Df}\right)^2. \tag{5}$$

C_{EA} represents the variation of the effect of the added mass of fluid with the response, taking into account not only the lift term in phase with the acceleration of the body, but also the amplitude and frequency of the response for each reduced velocity. As seen in figure 12b, the effective added mass for the wavy cylinders is comparable to that observed for the plain cylinder under VIV.

Obviously, if $C_y \cos\phi$ and C_{EA} were derived directly from $\tilde{C}_y$ and ϕ, which presented similar trends for the three models, one should not expect different behaviors between them in the results

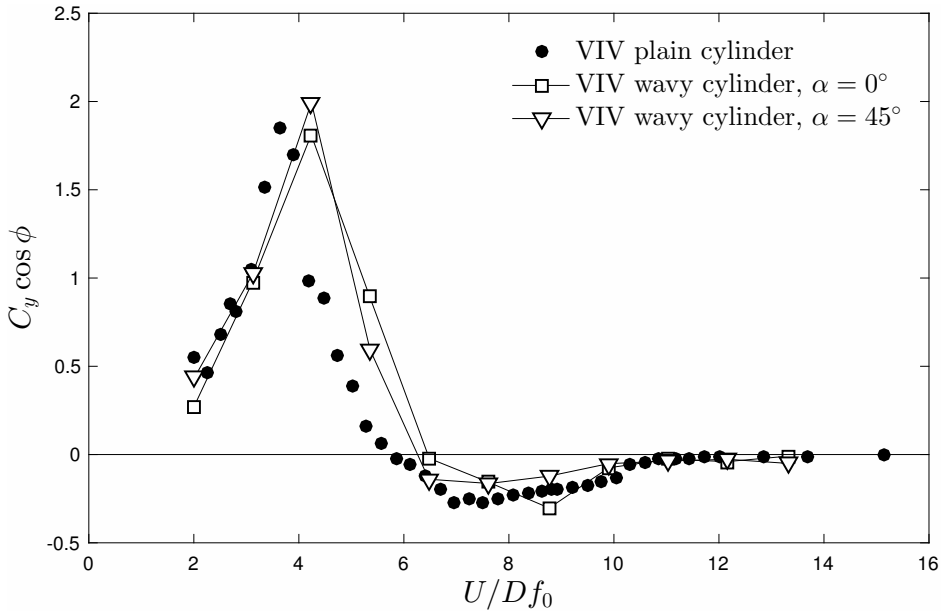

(a)

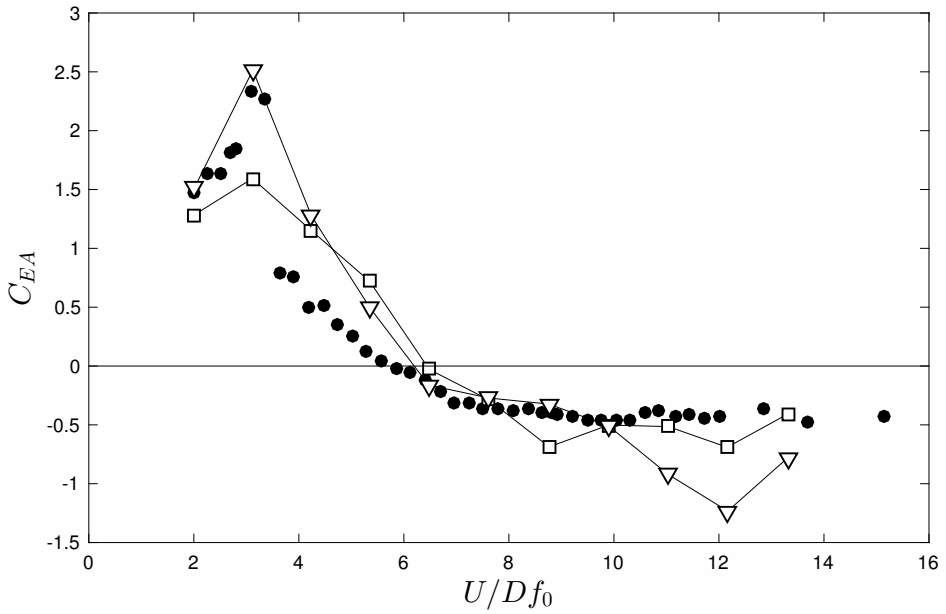

(b)

Figure 12: *(a)* Lift coefficient in phase with body acceleration and *(b)* effective added mass coefficient.

of figure 12. Nevertheless, figure 12 offers clear evidence that the effect due to the added mass of fluid in not significantly different for the wavy cylinder when compared with the plain cylinder. We conclude that, once the cylinders are oscillating, the three-dimensional surface of the wavy cylinder cannot produce any significant different fluid-dynamic effect than that produced by the movement of a plain cylinder.

Figure 13a, presenting the lift term in phase with the body velocity, also supports that conclusion. $C_y \sin\phi$ takes the form of a "negative fluid-dynamic damping", injecting energy into the system to sustain the vibrations. Results for the wavy cylinder are very similar to those of the plain cylinder. The energy transferred from the flow to the body in one cycle of oscillation is defined by

$$E = \pi \frac{\hat{y}}{D} C_y \sin\phi, \tag{6}$$

and presented in figure 13b against reduced velocity. We may conclude that the hydroelastic mechanism exciting the elliptic wavy cylinders into vibration is indeed the same as the one that excites the plain cylinder into VIV.

Now, if the excitation coming from the flow is the same in both cases (either with a plain or with our wavy cylinders), the dominant flow structures in the near wake should be similar between the two cases too. As mentioned in the literature review presented in the introduction, we know that the 3D surface of the wavy cylinder may disrupt the near wake of a fixed body (changing the separation lines, thus reducing drag). But it seems that once the body is free to oscillate, the dynamics of the wake is affected in such a way that the dominant mechanism is roughly the same for the plain cylinder and for the wavy cylinders.

We shall now turn to investigate the dominant flow structures of these cases by describing flow visualizations of the near wake.

4. Three-dimensional wake structure

As mentioned before, the near wake of a wavy cylinder is affected by the 3D shape of the surface. Most of the time, the characteristic wavelength of the surface appears in the dominant flow structures developing in the near wake. The separation lines on both sides of the bluff body are affected by the 3D shape of the surface, interfering with the behavior of the free shear layers which alters the width and length of the near wake. The axial-type of vortex filaments that characterize

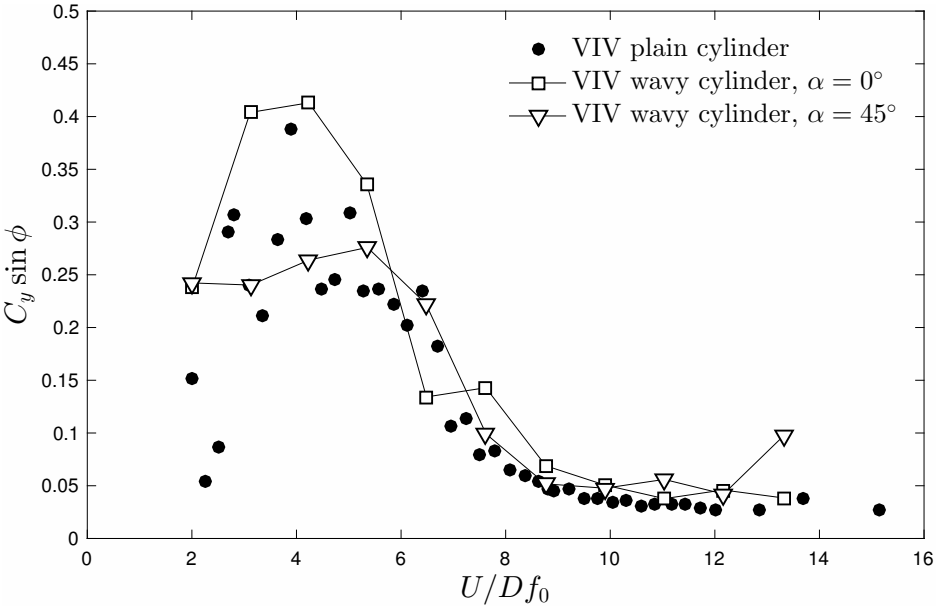

(a)

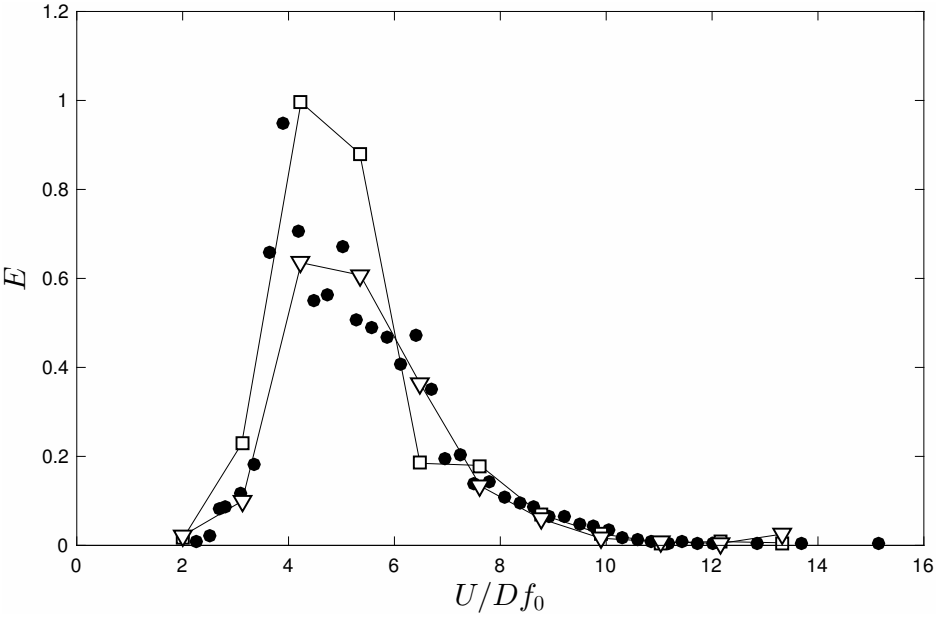

(b)

Figure 13: *(a)* Lift coefficient in phase with body velocity and *(b)* energy transferred from flow to structure during one cycle of vibration.

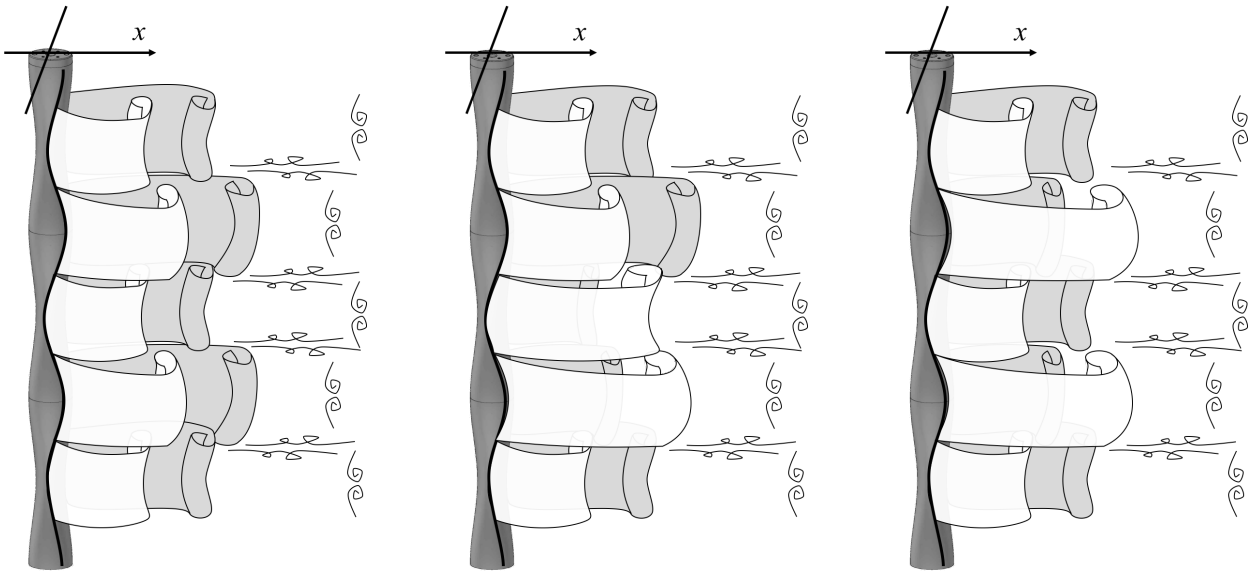

(a) (b) (c)

Figure 14: Examples of three-dimensional wake patterns for a fixed wavy cylinder.

the Kármán wake may still be the dominant flow feature, but longitudinal vortices appear at regular intervals related to the wavelength of the body geometry. This was observed to occur for various types of wavy cylinders and other bluff geometries with sinusoidal surfaces.

4.1. Fixed cylinder at $\alpha = 0^\circ$

Figure 14 illustrates possible 3D patterns observed in the near wake of a fixed wavy cylinder. When the body was not moving, the separation line presented a very three-dimensional shape following the saddle and node curvatures of the surface. The separation lines are represented in figure 14 by a solid black line along the body. The separation was delayed near the saddle regions and advanced near the nodes, extending or reducing the reach of the free shear layers before they rolled up to form coherent vortices.

Sometimes, the axial vortex filaments (z-vorticity, aligned with the axis of the body) appeared well correlated along the span for various cycles of vortex shedding, as illustrated in figure 14a. An undulation of the vortex filaments at the characteristic wavelength of the surface was noticeable, with streamwise vortices appearing at regular intervals further downstream (these are represented by curled black lines), but still a coherent vortex filament was visualized. Other times, as illustrated in the example of figure 14b, the axial vortex filament on one side appeared uncorrelated along

the span, which also resulted in stronger three-dimensional vortices in the x and y direction in the wake (represented by the curled lines). Still at other times, as illustrated in figure 14c, for a few shedding cycles, the axial vortex filaments appeared to be "broken", alternating shorter and longer vortex-formation lengths associated with the saddle and node regions of the body. Much stronger three-dimensional vortices appeared in the wake, contributing to dissipate the bubbles rather quickly.

In summary, the coherent axial vortex filaments could take many disturbed shapes, but always followed the wavelength characteristic of the surface of the body. As a general rule, axial vortices generated near the nodes were formed closer to the base of the cylinder, while vortices generated near the saddles were developed further downstream. Vortices in the x direction were observed to form near the node regions. As a consequence, vortical structures in the y direction were intensified further downstream in the turbulent wake, which is rich in three-dimensionalities. This is in good agreement with the observations of Lam et al. (2004b) and Zhang et al. (2005). The wake pattern illustrated in figure 14a was the most common, sustained during most of the shedding cycles.

The reader should bear in mind that the representation of vortices in figures 14 and 15 are simply an illustration to emphasize the dominant features of the wake. Obviously, vortex filaments cannot end in the fluid and vortex sheets cannot be abruptly interrupted as the image may suggest. The impression of a discontinuity between the vortex filaments is not real; the intricate 3D structures of smaller scales are too complex to be detailed in these flow sketches. Our objective with these artworks is to emphasize the correlation between the separation lines and possible dominant flow structures observed in the wake.

4.2. Oscillating cylinder at $\alpha = 0°$

Once the wavy cylinder was allowed to oscillate under VIV, the wake pattern was considerably changed. Figure 15a repeats the illustration of the dominant wake structure for a fixed wavy cylinder as a reference. The same pattern was only observed to occur for very small responses, below $\hat{y}/D = 0.1$, therefore only occurring at U/Df_0 less than 2.5 or greater than 11 (even though visualization was difficult at higher Re). The separation lines were closely sinusoidal (represented by a solid black line on the surface), following the saddle and node curvatures in the cross-flow and streamwise directions, as illustrated.

As the response increased slightly above $\hat{y}/D = 0.1$ for $U/Df_0 = 3$, the lateral movement of

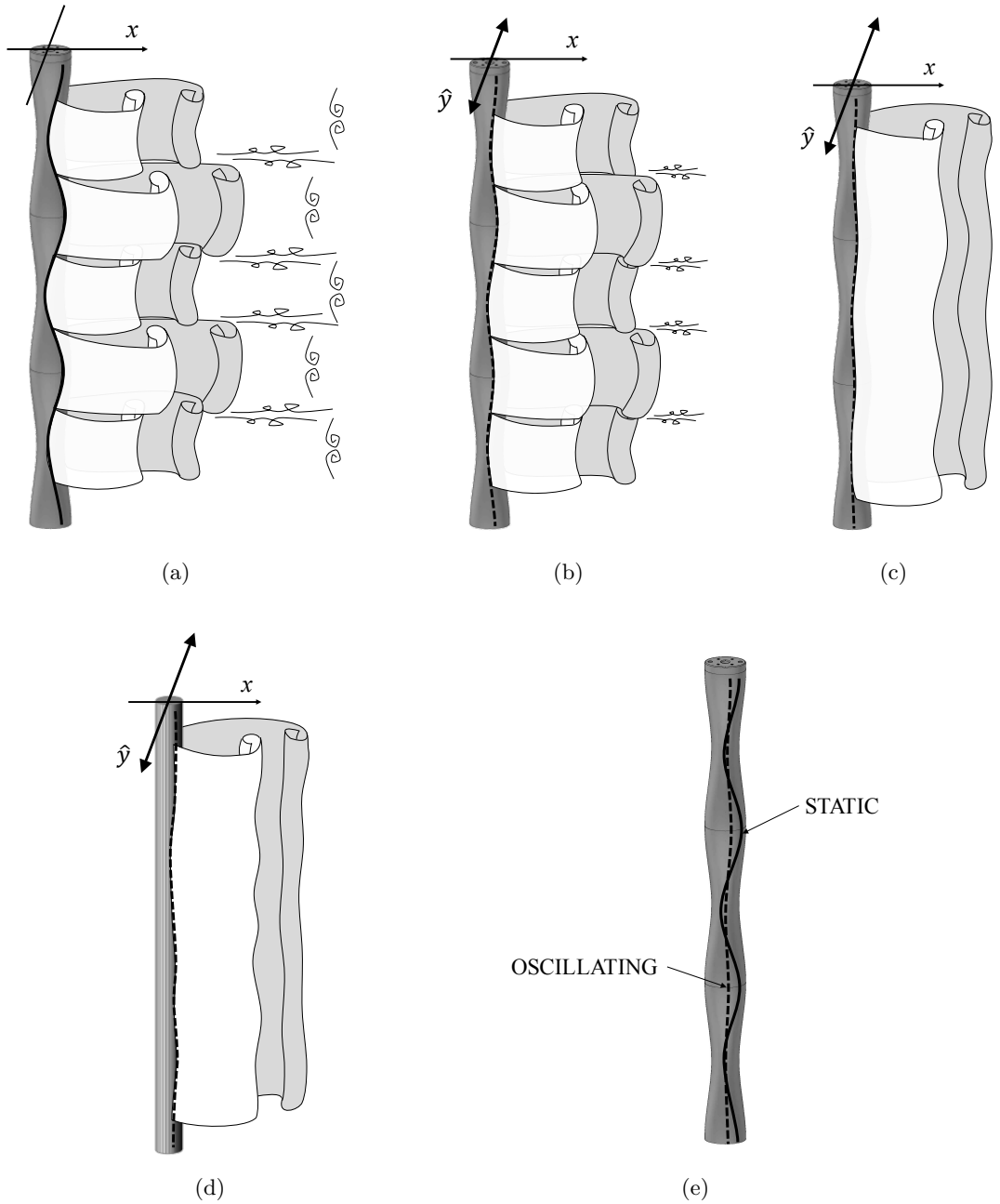

Figure 15: 3D wake patterns: *(a)* static wavy cylinder, *(b)* wavy cylinder at low $\hat{y}/D$, *(c)* wavy cylinder at high $\hat{y}/D$, *(d)* oscillating plain cylinder. *(e)* Sketch of separation lines on a wavy cylidner.

the cylinder started to affect the separation lines, as seen in figure 15b. As their shape became less sinusoidal (represented by a dashed black line), the axial vortex filaments in the near wake straightened up. Vortices in the x and y directions were reduced in strength.

Finally, in figure 15c, as the response reached its maximum value of $\hat{y}/D = 0.8$ for $U/Df_0 \approx 5$, the separation lines became fully correlated along the span, featuring an almost perfect straight line along the wavy surface (dashed black line). The axial vortex filaments recovered a degree of correlation that resembled that seen for the vortex filaments of an oscillating plain cylinder, illustrated in figure 15d for comparison. Consequently, the wake structure became closely two dimensional, with no sign of a characteristic wavelength appearing in the distribution of streamwise vortices.

As summarized in figure 15e, it appeared that only a small lateral movement of the wavy cylinder was necessary for the sinusoidal separation lines found on the fixed body to correlate along the span. The 3D flow structures induced by the waviness of the surface were thus replaced by a coherent wake of almost parallel vortex filaments.

4.3. Sectional wake patterns for $\alpha = 0^\circ$ and 45°

What happened for a wavy cylinder at $\alpha = 45^\circ$ was not very different. As one can now imagine, if the lateral oscillation is able to recorrelate the separation lines over the wavy surface, the variation of angle of attack should not be an obstacle. Figure 16a presents a simple diagram illustrating the vortex-shedding mechanism of a plain circular cylinder. This will serve as a reference to compare wake width and vortex-formation length.

Figure 16b illustrates the vortex-shedding mechanism for a fixed and an oscillating wavy cylinder at $\alpha = 0^\circ$ drawn at 2D planes along the span. For a fixed cylinder, the wake was narrower and longer at the saddle (station 0) and wider and shorter at the node ($P/2$). The circular section at $P/4$ represents the transition from one pattern to the other. It was near this region, although a bit closer to the node, that the streamwise vortices appeared (represented by curled dashed lines). If the cylinder was oscillating, as seen in the diagram to the right, the wake regained its correlation and very little difference was noticed between flow structures near saddle and nodes (maybe only a small variation in wake width), but a considerable variation in the vortex-formation length. The same features were observed by Wang and Liu (2016), who performed time-resolved particle-image velocimetry of the flow around a seal whisker with similar wavy morphology.

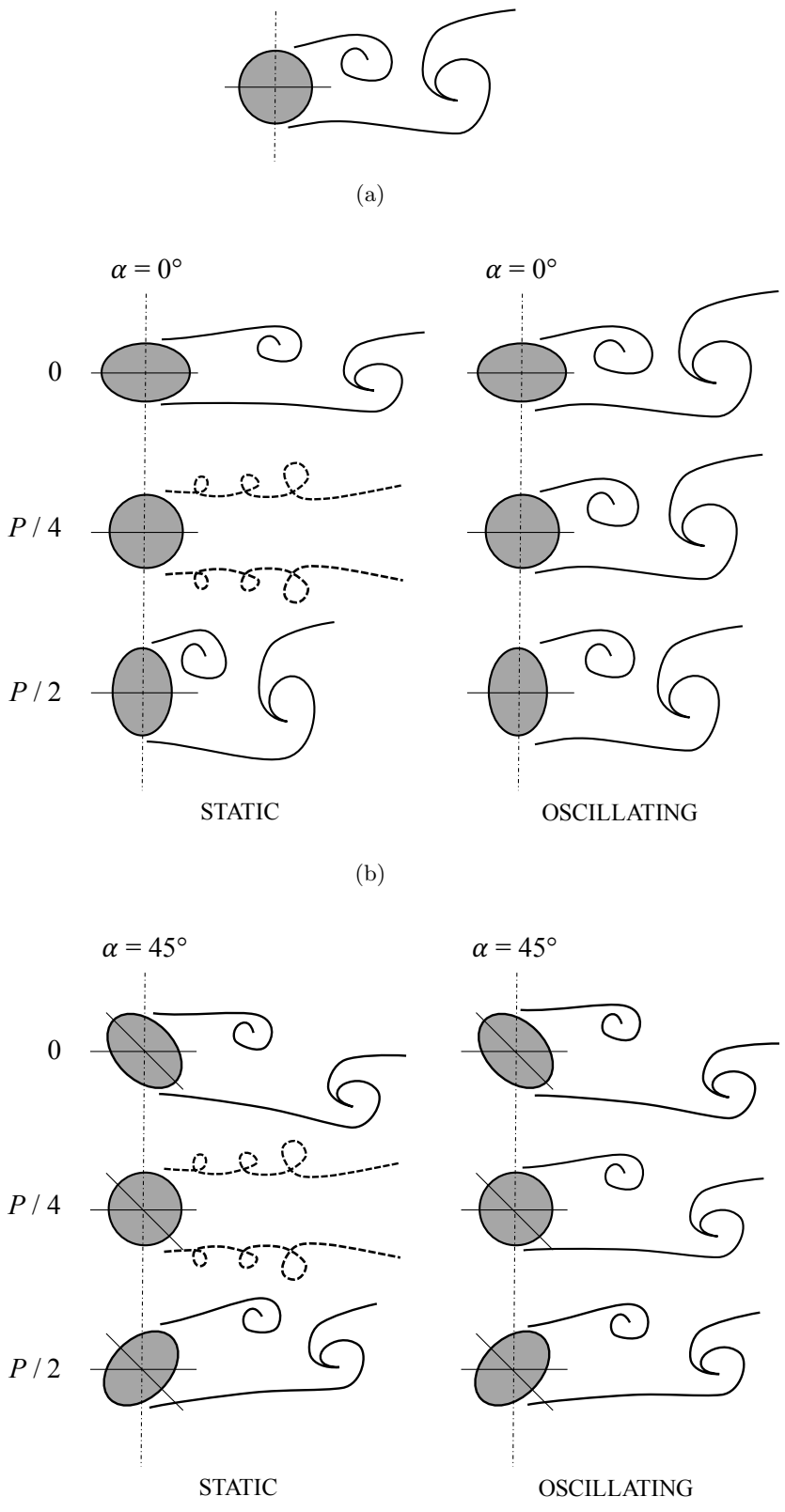

Figure 16: Sectional wake patterns for fixed and oscillating cylinders: *(a)* plain cylinder, *(b)* wavy cylinder at $\alpha = 0^\circ$, *(c)* wavy cylinder at $\alpha = 45^\circ$.

For the wavy cylinder at $\alpha = 45°$, illustrated in figure 16c, the same pattern was observed with only minor variations occurring between the saddle and the node. Now that the fixed wavy cylinder faced the flow at an incidence angle at stations 0 and $P/2$, the wake at these regions was slightly inclined following the more elongated shape of the elliptic cross section. However, once the body started to oscillate (as seen on the right), the angle of incidence was barely noticed by the flow and a spanwise correlated wake appeared once more.

5. Final remarks

The differences in curvatures between saddles and nodes are more accentuated for elliptical cross sections and could intensify the 3D characteristics of the wake that favour drag reduction. We have verified the observations of Bearman and Owen (1998), who stated that reductions in drag can be achieved when the separation lines on a fixed bluff body are forced to be sinuous. However, once the body started to oscillate in the cross-flow direction, the separation lines on the sides of the wavy cylinder straightened up, recovering the shedding of vortices forming a wide Kármán wake. This observation is in agreement with the findings of Zhang et al. (2017), who performed numerical simulations for a free-to-oscillate wavy cylinder with circular cross sections. As shown by Blackburn (1998), the lateral oscillation has a tendency of straightening up the separation lines of a plain cylinder.

In general, we suggest the same occurs for a three-dimensional cylinder if the 3D features of the surface are not sufficiently pronounced to hold the sinuous separation lines in place. As a consequence, the elastic body will be able to pick up even the minute excitation from the flow acting near its resonant frequency, thus enhancing the response. If the level of mass and damping in the system is high enough, the initial excitation resulting from sinuous separation lines might not be strong enough to overcome the loss of energy due to damping, thus vibration will not develop. But for systems with a low mass-damping parameter, an initial perturbation may result in a large enough lateral movement that could in turn realign the separation lines.

This shows that the physical mechanisms driving the VIV of the wavy cylinder are not different in nature from those occurring with the plain cylinder. Response curves and a detailed analysis of fluid forces discussed above support that conclusion. When the bodies are oscillating, the separation lines for the wavy cylinder recover a less 3D shape, similar to that on a plain cylinder.

We argue that sharp 3D perturbations are required to hold the separation lines in a 3D shape. Helical strakes, for example, have distinctively pronounced features in the form of sharp helical blades. It is very difficult for the flow to modify the 3D separation lines fixed by the high blades. Small vibrations would not be enough. If the height of the strake is not high enough, it might be that a small lateral movement of the body results in a roughly straight separation line on the side. Therefore, significantly higher strakes are required to suppress VIV of low mass-damping system (immersed in water, for example) than of high mass-damping systems (immersed in air, such as chimneys and cables). But if the strakes are high enough, the separation lines follow the shape of that sharp geometry, interfering with the flow. The setback, however, is the amount of drag generated. In order to hold the 3D separation lines along the span, the larger strakes will generate considerably more drag.

Therefore we argue that a combination of VIV suppression and significant drag reduction is very difficult to be achieved (if not impossible) for low mass-damping systems. Smooth three-dimensional surfaces that would generate considerably less drag (such as the present wavy cylinder) are not efficient in fixing the sinuous separation lines required to reduce the excitation. Sharp-edged surfaces might still hold the separation lines under small lateral movements, but they increase drag as a consequence.

On the other hand, this hydroelastic behavior might be useful for the seals whose whiskers have a very similar geometry, as reported by Beem and Triantafyllou (2015). Out of the synchronization range of VIV the whisker would present insignificant vibration with minimal drag. However, once the whisker is triggered to vibrate — say by turbulence buffeting or by a sudden pressure fluctuation in the upstream flow coming from the wake of a swimming fish — the initial movement would be enough to cause the realignment of the separation lines, enhancing the response. This mechanism would produce a drag-efficient whisker with augmented capacity to respond with flow-induced vibrations to perturbations in the upcoming flow.

Of course the dynamic response of a seal whisker would be different from that observed for this idealized case with a rigid cylinder. The whisker would probably present higher mass and structural damping than our cylinder. Also, the flexible whisker would be deflected by the flow as a cantilever beam, responding with vibrations in both inline and cross-flow directions (not to mention the possibility of higher modes of vibration). Nevertheless, we hope that our data acquired

in an idealized experiment with a rigid wavy cylinder with low mass and damping responding in one degree of freedom will help the study of marine mammals and support the development of other bioinspired applications.

6. Conclusion

From the present experimental investigation we can conclude that a wavy cylinder with the level of three-dimensional surface variation proposed herein developed vortex-induced vibrations with the same behavior seen for a plain cylinder with equivalent diameter. A fixed wavy cylinder indeed presented reduced drag when compared to a plain cylinder (an average reduction of about 12.5%). The modified regions of an elongated wake with substantial 3D flow features increased the base pressure and improved the performance as far as drag is concerned.

The 3D features of the elliptical wavy cylinder are more prominent than those of a wavy cylinder with circular cross section (of equivalent mean diameter). However, once the body responded in the cross-flow direction, the separation lines of the wavy cylinder straightened up, recovering a wide Kármán wake. We conclude that the three-dimensional separation lines on a wavy cylinder were correlated by the lateral movement of the body responding to flow-induced excitations, hence the hydroelastic mechanism that drives the wavy cylinder into VIV is not different from that of a plain cylinder.

Aknowledgements

The original research work on the development of VIV suppressors was sponsored by BP Exploration Operating Company Ltd. GRSA acknowledges the support of FAPESP (2011/00205-6, 2014/50279-4), CNPq (306917/2015-7) and the Brazilian Navy.

References

Ahmed, A., 2010. On the wake of a circular cylinder with nodal and saddle attachment. Journal of Fluids and Structures 26 (1), 41 – 49.

Ahmed, A., Bays-Muchmore, B., 1992. Transverse flow over a wavy cylinder. Physics of Fluids A 4 (9), 1959–1967.

Assi, G. R. S., Bearman, P. W., Carmo, B., Meneghini, J., Sherwin, S., Willden, R., 2013. The role of wake stiffness on the wake-induced vibration of the downstream cylinder of a tandem pair. J. Fluid Mech. 718, 210–245.

Assi, G. R. S., Bearman, P. W., Kitney, N., 2009. Low drag solutions for suppressing vortex-induced vibration of circular cylinders. J. Fluids Structures 25, 666–675.

Assi, G. R. S., Bearman, P. W., Kitney, N., Tognarelli, M., 2010a. Suppression of wake-induced vibration of tandem cylinders with free-to-rotate control plates. J. Fluids Structures 26, 1045–1057.

Assi, G. R. S., Bearman, P. W., Meneghini, J., 2010b. On the wake-induced vibration of tandem circular cylinders: the vortex interaction excitation mechanism. J. Fluid Mech. 661, 365–401.

Assi, G. R. S., Franco, G. S., Vestri, M. S., 2014. Investigation on the stability of parallel and oblique plates as suppressors of vortex-induced vibration of a circular cylinder. Journal of Offshore Mechanics and Arctic Engineering 136 (3), 031802–031802–9.

Bearman, P. W., 1984. Vortex shedding from oscillating bluff bodies. Annu. Rev. Fluid Mech. 16, 195–222.

Bearman, P. W., Brankovic, M., 2004. Experimental studies of passive control of vortex-induced vibration. European Journal of Mechanics - B/Fluids 23 (1), 9 – 15.

Bearman, P. W., Owen, J. C., 1998. Reduction of bluff-body drag and suppression of vortex shedding by the introduction of wavy separation lines. Journal of Fluids and Structures 12 (1), 123–130.

Beem, H. R., Triantafyllou, M. S., 11 2015. Wake-induced 'slaloming' response explains exquisite sensitivity of seal whisker-like sensors. Journal of Fluid Mechanics 783, 306–322.

Bell, W., 1983. Turbulence vs drag—some further considerations. Ocean Engineering 10 (1), 47 – 63.

Blackburn, H. M., 1998. A comparison of two- and three-dimensional wakes of an oscillating circular cylinder. In: 13th Australasian Fluid Mechanics Conference. pp. 749–752.

Cai, J., Chng, T. L., Tsai, H. M., 2008. On vortical flows shedding from a bluff body with a wavy trailing edge. Physics of Fluids 20 (6).

Cicolin, M. M., Assi, G. R. S., 2017. Experiments with flexible shrouds to reduce the vortex-induced vibration of a cylinder with low mass and damping. Applied Ocean Research (in press), Doi: 10.1016/j.apor.2017.04.003.

Darekar, R., Sherwin, S., 2001. Flow past a bluff body with a wavy stagnation face. Journal of Fluids and Structures 15 (3), 587 – 596.

Gerrard, J., 1966. The mechanics of the formation region of vortices behind bluff bodies. J. Fluid Mech. 25, 401–13.

Ginter, C. C., Fish, F. E., Marshall, C. D., 2010. Morphological analysis of the bumpy profile of phocid vibrissae. Mar. Mammal Sci. 26, 733.

Gioria, R. S., Carmo, B. S., Meneghini, J. R., 2007. Three dimensional wake structures of flow around an oscillating circular cylinder. In: ASME 2007 26th International Conference on Offshore Mechanics and Arctic Engineering. American Society of Mechanical Engineers, pp. 833–839.

Hanke, W., Witte, M., Miersch, L., Brede, M., Oeffner, J., Michael, M., Hanke, F., Leder, A., Dehnhardt, G., 2010. Harbor seal vibrissa morphology suppresses vortex-induced vibrations. Journal of Experimental Biology 213 (15), 2665–2672.

Hans, H., Miao, J. M., Triantafyllou, M. S., 2014. Mechanical characteristics of harbor seal (phoca vitulina) vibrissae under different circumstances and their implications on its sensing methodology. Bioinspiration & Biomimetics 9 (3), 036013.

Hover, F. S., Davis, J. T., Triantafyllou, M. S., 2004. Three-dimensionality of mode transition in vortex-induced

vibrations of a circular cylinder. European Journal of Mechanics - B/Fluids 23 (1), 29 – 40.

Jung, J. H., Yoon, H. S., 11 2014. Large eddy simulation of flow over a twisted cylinder at a subcritical reynolds number. Journal of Fluid Mechanics 759, 579–611.

Khalak, A., Williamson, C. H. K., 1999. Motions, forces and mode transitions in vortex-induced vibrations at low mass-damping. J. Fluids Structures 13, 813–851.

Kim, W., Lee, J., Choi, H., 2016. Flow around a helically twisted elliptic cylinder. Physics of Fluids 28 (5).

Kleissl, K., Georgakis, C., 2011. Aerodynamic control of bridge cables through shape modification: A preliminary study. Journal of Fluids and Structures 27 (7), 1006 – 1020.

Lam, K., Lin, Y. F., 2009. Effects of wavelength and amplitude of a wavy cylinder in cross-flow at low reynolds numbers. Journal of Fluid Mechanics 620, 195–220.

Lam, K., Wang, F., Li, J., So, R., 2004a. Experimental investigation of the mean and fluctuating forces of wavy (varicose) cylinders in a cross-flow. Journal of Fluids and Structures 19 (3), 321 – 334.

Lam, K., Wang, F., So, R., 2004b. Three-dimensional nature of vortices in the near wake of a wavy cylinder. Journal of Fluids and Structures 19 (6), 815 – 833.

Lee, S.-J., Nguyen, A.-T., 2007. Experimental investigation on wake behind a wavy cylinder having sinusoidal cross-sectional area variation. Fluid Dynamics Research 39 (4), 292.

Nakamura, H., Igarashi, T., 2008. Omnidirectional reductions in drag and fluctuating forces for a circular cylinder by attaching rings. Journal of Wind Engineering & Industrial Aerodynamics 96 (6-7), 887–899.

New, T. H., Shi, S., Liu, Y., 2013. Cylinder-wall interference effects on finite-length wavy cylinders at subcritical reynolds number flows. Experiments in Fluids 54 (10), 1601.

Owen, J. C., Bearman, P. W., Szewczyk, A. A., 2001. Passive control of VIV with drag reduction. J. Fluids Structures 15, 597–605.

Owen, J. C., Szewczyk, A. A., Bearman, P. W., 1999. Suppressing Karman vortex shedding by use of sinuous circular cylinders. In: APS Division of Fluid Dynamics Meeting Abstracts.

Owen, J. C., Szewczyk, A. A., Bearman, P. W., 2000. Suppression of kármán vortex shedding. Physics of Fluids 12 (9), S9–S9.

Rashidi, S., Hayatdavoodi, M., Esfahani, J. A., 2016. Vortex shedding suppression and wake control: A review. Ocean Engineering 126, 57–80.

Rinehart, A., Shyam, V., Zhang, W., 2017. Characterization of seal whisker morphology: implications for whisker-inspired flow control applications. Bioinspiration & Biomimetics 12 (6), 066005.

Silva-Ortega, M., Assi, G., 2017. Flow-induced vibration of a circular cylinder surrounded by two, four and eight wake-control cylinders. Experimental Thermal and Fluid Science 85, 354 – 362.

Wang, S., Liu, Y., 2016. Wake dynamics behind a seal-vibrissa-shaped cylinder: a comparative study by time-resolved particle velocimetry measurements. Experiments in Fluids 57 (3), 32.

Williamson, C., 1996. Vortex dynamics in the cylinder wake. Annual Review of Fluid Mechanics 28 (1), 477–539.

Williamson, C. H. K., Govardhan, R., 2004. Vortex-induced vibrations. Annu. Rev. Fluid Mech. 36, 413–55.

Zdravkovich, M. M., 1981. Review and classification of various aerodynamic and hydrodynamic means for suppressing vortex shedding. J. Wind Eng. Industrial Aerodynamics 7, 145–189.

Zdravkovich, M. M., 1997. Flow around circular cylinders, Volume 1, 1st Edition. Oxford University Press.

Zdravkovich, M. M., Brand, V. P., Mathew, G., Weston, A., 1989. Flow past short circular cylinders with two free ends. Journal of Fluid Mechanics 203, 557–575.

Zhang, K., Katsuchi, H., Zhou, D., Yamada, H., Han, Z., 2016. Numerical study on the effect of shape modification to the flow around circular cylinders. Journal of Wind Engineering and Industrial Aerodynamics 152, 23 – 40.

Zhang, K., Katsuchi, H., Zhou, D., Yamada, H., Zhang, T., Han, Z., 2017. Numerical simulation of vortex induced vibrations of a flexibly mounted wavy cylinder at subcritical reynolds number. Ocean Engineering 133 (Supplement C), 170 – 181.

Zhang, W., Daichin, Lee, S. J., 2005. PIV measurements of the near-wake behind a sinusoidal cylinder. Experiments in Fluids 38 (6), 824–832.